UNIVERSIDADE DA BEIRA INTERIOR
Engenharia

Space Tether Systems
Uniform Rotations of a Dumbbell-like System

Simão António da Rocha e Brito de Aguiã Morant

Dissertação para obtenção do Grau de Mestre em
Engenharia Aeronáutica
(Ciclo de Estudos Integrado)

Orientador: Prof. Doutora Anna D. Guerman
Co-orientador: Prof. Doutor Denilson P. S. dos Santos
Co-orientador: Prof. Doutor Pedro V. Gamboa

Covilhã, Junho 2014

Left blank

Dedication

I would like to dedicate this work to a few special people to whom I'm really thankful:

To my girlfriend Joana, who had to endure my bad temper in my sleepless nights and never-ending days.

To my parents, who believed me and made me believe.

To Prof. Denilson Santos and his wife Heliene, who have accompanied me tirelessly in my work, and to whom I'm grateful for all the attention they had with me. I will never forget the siri dance that inspired me with laughs through the last months.

And at last, but not least, Prof. Anna Guerman, who kindly guided me and offered me the possibility to work in a field where dreams are beyond the sky.

Left blank

Acknowledgment

I am grateful to Fundação para a Ciência e a Tecnologia, who offered me a research grant in the context of this dissertation, and to Prof. Anna Guerman, who made this grant possible.

Left blank

Abstract

In this dissertation, a dumbbell-like system is analyzed, considering two mass points connected by a massless and rigid tether with variable length; its center of mass moves along an elliptic Keplerian orbit. This kind of a system, in a certain type of configurations, is a simple conceptualization of a space elevator. The system motion is obtained using the Lagrangian formulation in a central gravitational field. The laws of control are considered for the system's rotation around its center of mass; those include the uniform rotations or permanent orientation with respect to the local vertical. The stability conditions are obtained for the first case, analyzing the equation in variations and using the Floquet theory. The results show that there are regions of eccentricities where stability is found. Lastly, a dynamic numerical simulator is created, where the implementation of the results can be tested.

Key-words

Tether Systems, Space Elevator, Dumbbell-like System, Stability of Solutions, Floquet Theory, Monodromy Matrix.

Left blank

Resumo

Nesta dissertação, um sistema tipo halteres é analisado, considerando dois pontos de massa conectados com um cabo rígido, sem massa e com variações do comprimento, e com o centro de massa movendo-se segundo uma órbita Kepleriana. Este tipo de sistema, num certo tipo de configuração, é uma simples conceptualização do elevador espacial. O movimento do sistema é obtido com recurso à Formulação Lagrangiana num Campo Gravitacional Central. As leis de controlo são consideradas para uma rotação do sistema à volta do seu centro de massa. Essas incluem rotações uniformes e uma orientação permanente. As condições de estabilidade para o primeiro caso foram obtidas, analisando a respectiva equação em variações e utilizando a Teoria de Floquet. Os resultados mostraram que existem intervalos dos valores de excentricidade onde a estabilidade é encontrada. Por último, um simulador numérico e dinâmico foi criado, para se testar a implementação destes resultados.

Palavras-chave

Sistemas Ligados por Cabos, Elevador Espacial, Sistema Tipo Halteres, Estabilidade, Teoria de Floquet, Matriz de Monodromia.

Left blank

Index

Left blank

List of Figures

List of Tables

Left blank

List of Acronyms

UBI	Universidade da Beira Interior
TSS	Tethered Satellite System
CG	Center of Gravity
CM	Center of Mass
ISS	International Space Station
e	Eccentricity
ν	True anomaly
φ	Angle of rotation of the system around the center of mass
V	Potential Energy
T	Kinetic Energy
l	Tether length
l_0	Initial tether length
l_i	Length from the center of mass to point i
m_i	Mass of point i

Left blank

Chapter 1 - Introduction

Nowadays, we foresee the future of our civilization as a high-tech society, where the space journey makes part of our quotidian life. A society like that needs some robust infrastructures that make possible the transport of merchandise and people. Space elevator is one of the best options available, since it does not need rockets to reach space. Compared with rocket propulsion [1], as V. Kaithi wrote, "the space elevator can provide easier, safer, faster and cheaper access to space exploration".

An Earth space elevator is a transport system composed by a long tether, connecting Earth and a ballast in a geostationary orbit. The cable will have to be very strong, since it will have some physical challenges, as referred in Section 2.2. Despite those difficulties, the advances in materials like carbon fibers do make this elevator possible, at least to be considered. Even though we will not surely see this structure in the next years, there are being made interesting analysis, studying the different aspects of such giant structure and developing technologies to accomplish the main objective.

Artificial satellites have been suggested to launch the tether. The cable will start downwards, from a geostationary orbit, and falling into Earth – in some point in the Equatorial line. To conceptualize some missions, it is important to study the dynamics of such systems, and ensure stability is achieved.

Figure 1.1 Artist Concept of a Space Elevator, from NASA Online Image Gallery

1.1 General Purpose

Since 1960th several researchers have been studying the possibilities to control attitude motion of space systems with variable mass distributions with the intention to control spacecraft dynamics. One of the purposes of this control can be implementation of a specific attitude motion required by the mission and stabilization of such motion with respect to perturbations. Here we consider dynamics of a two-body tether systems in a central Newtonian gravitational field. The perturbations of motion can occur for several factors, such as atmospheric drag, solar pressure, tether deployment, n-body perturbations, among others which are not discussed here. We assume that the center of mass of the system moves along a Keplerian orbit and study attitude dynamics, control, and stability of such dumbbell-like configuration. The motion's equation is written using Lagrangian formulation writing down the Kinetic and Potential Energy, and considering the possibility to control the tether length to implement a specific rotation around the system's center of mass. We also present a numerical simulator created for this goal.

Chapter 2 - Literature Review

2.1 Historical Perspective

In 1895, the Eiffel tower became the inspiration for Konstantin Tsiolkovsky. The Russian scientist dedicated his life to the study of astronautics and rocket physics and, encouraged by the tower, saw the opportunity to explore the outer space with the edification of a structure that could reach the space. That structure, in Tsiolkovsky idea, would have a tether in the top of it and it would extend for kilometers [2].

Although it seems a science fiction, just like in more than 80 sci-fi books and movies where such space tower appears, , since the 1980s scientists have performed several studies to evaluate a real scenario for space elevator (see, e.g., Swan and Swan [3]).

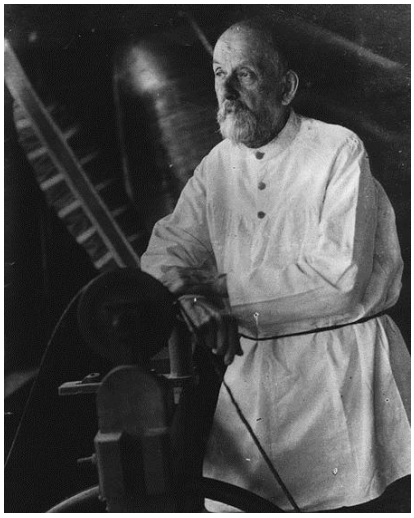

Figure 2.1 Konstantin Tsiolkovsky

2.2 The general concept

The first concept of a Space Elevator, as referred previously, is based on Tsiolkovksy's idea. He regarded some problems mostly concerned with the structure itself. According to [4] some of these problems were:

- The tether material;
- The susceptibility to vibrations;

- The wobble from Coriolis force;
- The space debris;
- Social and Environmental Risks;
- Collisions with meteoroids and micrometeorites;
- Corrosion;
- Radiation and consequent ionization.

The concept proposed by Edwards and Westling [5] consists in one long tether of about 1 meter in width and of an insignificant thickness (macromolecules size), attached to Earth and extending to the outer space. Figure 2.2.1 shows the concept and the deployment phases of the space elevator.

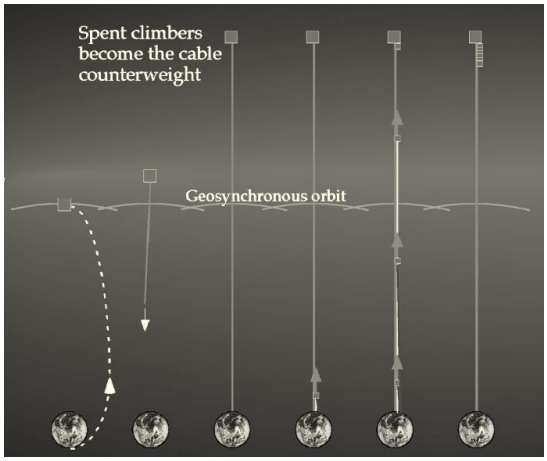

Figure 2.2.1 Deployment overview scheme from Bartoszek Engineering

2.3 Applications and missions of tethers in space structures

To understand the concept of a space elevator, it is important to comprehend the dynamics of space systems connected with tethers. Space tether systems have been quite important in space exploration, since first applied in Gemini XI, in 1966. After that, the tethers have been used in several missions, providing passive attitude stabilization, while creating an artificial gravity and reducing the need to use the propellant.

As a matter of fact, there have been lots of applications attributed to the space tethers. The fundamental book of Beletsky and Levin [6] provides a review of a good amount of applications and makes an interesting analysis of the dynamics of space tether systems.

In [7], Cartmell and McKenzie focus on some interesting applications:

- Two-dimensional tethered constellations;
- Construction of a passive space facility with tethers separating platforms;
- Payload orbit raising and lowering;
- Elevator using tethers to the orbit transfers (from LEO to GEO);
- Tensions systems for solar sails.

Cosmo and Lorenzini [8] offer a good description of various applications. The list is very long including:

- Multiprobe for Atmospheric Studies
- Gravity Wave Detection Using Tethers
- Earth-Moon /Mars-Moon Tether Transport System
- Rotating Controlled-Gravity Laboratory
- Tethered Space Elevator
- Electrodynamic Power and Thrust Generation
- Communication Antenna
- Aerocapture with Tethers for Planetary Exploration
- Comet/Asteroid Sample Return
- Mars Tethered Observer
- Tethered Lunar Satellite for Remote Sensing
- (see Figures 2.3.1)

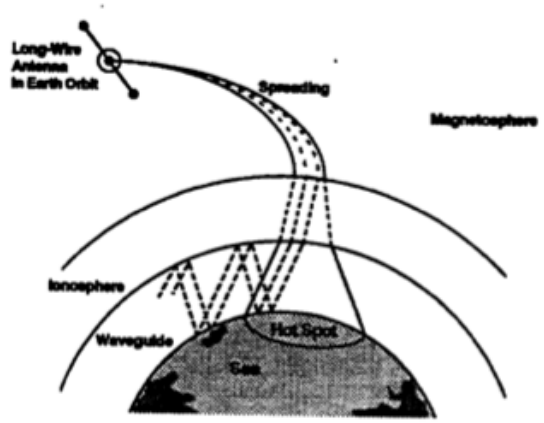

Figure 2.3.1.a Communication Antenna

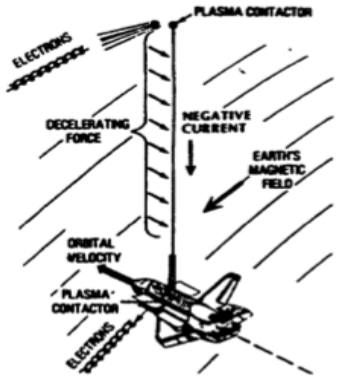

Figure 2.3.1.b Electrodynamic Power Generation

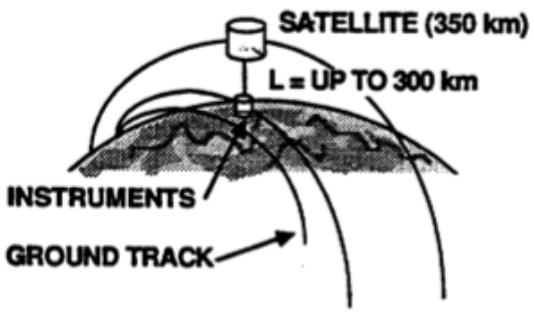

Figure 2.3.1.c Mars Observer

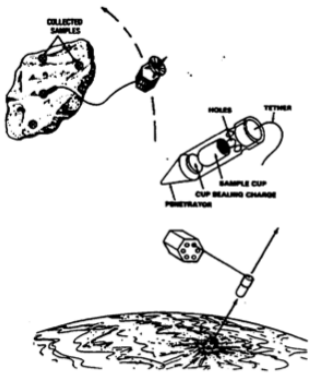

Figure 2.3.1.d Comet Sample Return

As listed above, tethers do have an important role in future space exploration. In formation flying systems, tethers are able to provide simple solutions to some problems of creating a convenient nominal motion, e.g., a state of equilibrium. As referred in [9] by M. v. Pelt, the different altitudes and the different time-launches of the satellites in formation or even the fact that the Earth is not perfectly round, make them to orbit in slightly different velocities, meaning they would drift away from each other, destroying therefore an intended formation configuration. Although the propulsion systems are still capable to correct the trajectory, they are limited and sometimes don't provide the required precision. Tethers offer a direct physical effect in the attitude control system, providing the means to the stabilization of the system. We focus in this subject in Section 2.4.

Some missions using TSS have been quite significant. As referred before, Gemini XI was the first one, using a tether to provide artificial gravity. John Hoffman et al. [10] analyze the dynamics of the tether to provide artificial gravity for the ASTOR (Advanced Safety Tether Operation and Reliability) project. In 1992, the mission Shuttle TSS-1 tested the TSS concept on the Space Shuttle, where the dynamics of TSS were evaluated [11] (see Figure 2.3.2). PMG mission successfully tested an electrodynamic tether [12], being able to convert electricity from orbital energy. In Table 2 [13] (see Annex 1) one can see numerous TSS missions. The same article explores all the mission's details. One important application conferred to space tether systems could be the use of net systems connected with tethers for debris capture and removal [14], as in 2010 the percentage of drift objects (space debris) in orbit around Earth were about 49% of the total.

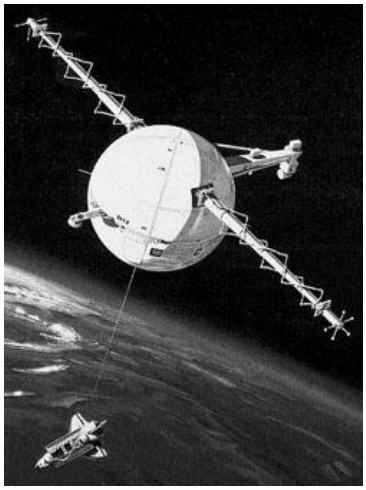

Figure 2.3.2 Shuttle TSS-1 Mission concept

2.4 Attitude Control

Attitude control, according to [15], refers to "maintenance of a desired, specified attitude within a given tolerance". Correctly determined, it allows the satellite system to be correctly oriented in the required orbit, giving some adjusts in its orientation over time and correcting perturbations. Those adjustments can be done in different ways:

- Spin stabilization;
- Momentum wheels;
- Control moment gyros;
- Solar sails;

- Gravity-gradient stabilizations;
- Etc.

The corrections in attitude usually need sensors for measuring the position in the orbit frame.

2.4.1 Gravity-gradient stabilization

Satellite tether systems can use the tether to provide gravity-gradient stabilization. This passive stabilization, also known as tidal stabilization, uses the appropriate body mass distribution and the gravitation field applied and does not require an active control system with sensors and actuators.

Consider a motion in a circular orbit of a simple dumbbell-like system, composed by two masses connected with a tether. When aligned with the local vertical, the two masses experiment different forces, as shown in Figure 2.4.1. The centrifugal force is larger in the upper element, but the gravitational force is weaker. On the contrary, the gravity force acting on the lower mass is larger, but the respective centrifugal force is weaker.

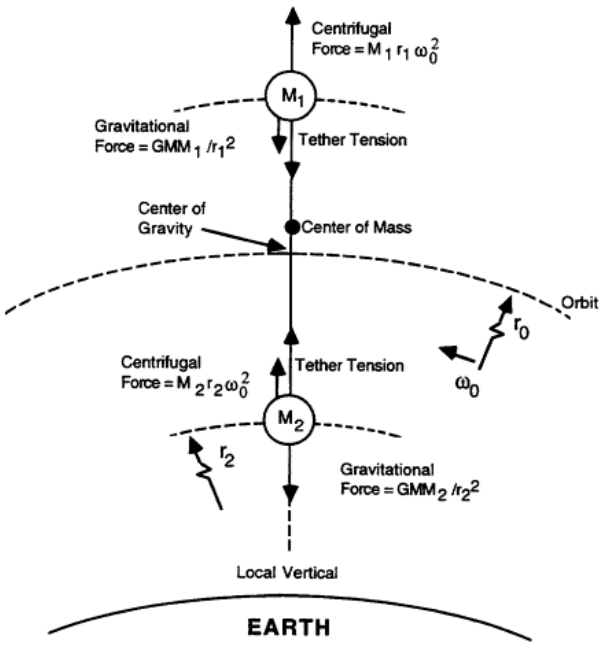

Figure 2.4.1 Acting forces on a dumbbell tether system

As one can notice (see, e.g., [8]), the resultant forces act on the system as a stabilization mechanism, forcing it into a vertical orientation. Therefore the system possesses two stable

equilibrium configurations, one shown in Figure 2.4.1, and the other inverse with respect to the local horizontal. (Note that for the case of a three-dimensional asymmetric rigid body, the same physical mechanism results in 24 equilibrium configurations, four of which are stable[1].)

The above example shows that for the motion in orbital environment the center of mass (cm) of the system normally doesn't coincide with its center of gravity (cg). Moreover, it is clear that the orbital motion of a large space system, such as a large tethered structure, cannot be separated from its attitude motion and therefore its orbit differs from the orbit of a point with the same mass (that is, from the respective Keplerian orbit). However, when the tether lengths are not too large, this difference is extremely small and will be neglected here.

2.5 State of the art

Some of the recent efforts done on the study of dynamic and control of space tethers systems show that the gravity-gradient is a natural and elegant solution to provide stabilization [10] [16]. However, some problems have been identified and referred to in several articles [17] [18] [19].

In [17], E.C. Lorenzini and J. Ashenberg note that the tether can be sometimes misaligned with respect to the local vertical at the center of mass. The orbital eccentricity itself produces small perturbations that influence the system stability. The same authors suggest an active stabilization mechanism based on the torque provided by the tether's tension. That mechanism can be implemented linking the tether to a rigid attachment fixed in the space station and adding a torque motor to it. This way, the torque is controlled actively. The authors developed a LQR (Linear Quadratic Regulator) controller taking into account the eccentricity of the Keplerian orbit, while the other papers at the time considered only circular orbits.

In [18] and [19], M. Pascal studies control laws for the tether deployment and retrieval. She states that in almost all studies, the law of deployment/retrieval is chosen "a priori" as linear or exponential law. The author combines different laws for fast and simple motions with analytical solutions for in-plane and out-of-plane motions, for massless and massive tethers and for circular and elliptical orbits. In the first article M. Pascal focuses on a crawler system, where a sub-satellite climbs the tether towards the Space Station, contrary to the notion of the tether being pulled to it. A scheme of a possible crawler system is represented in Figure 2.5.1 [20].

[1] P. C. Hughes, Spacecraft Attitude Dynamics. Dover Publications, 2004, 592 pp.

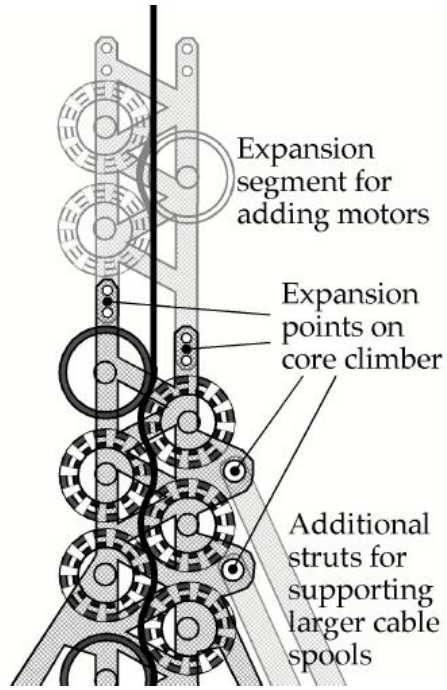

Figure 2.5.1 Crawler system

A. Djebli and M. Pascal deepen the study of advantages for the crawler system in [21], resulting in faster variation of the orbital parameters compared to conventional methods. The article suggests this system to attain orbital modifications. As a negative consequence, the change in absolute energy and the tether tension variations are higher than usual. A relevant adding are the radial and azimuthal accelerations trough Earth, causing some perturbations in the motion.

Some TSS state of the art applications have already been mentioned in Section 2.3. The review article of Cartmell & McKenzie [7] refers to the use of tethers as tension mechanisms in solar sail structures for trajectory corrections. An electrodynamic tether system can also create an artificial electric field, transferring momentum from charged particles of the solar wind to the system. The respective propulsion system e-sail (from solar wind electric sail, [22]) is already being tested in the ESTCube-1, ESA satellite. Tethers can also provide links for lower-altitude payloads and high-altitude solar sails and cube sails. An example of a cube sail is considered in [23], with a tether being a 260m long reflecting film. The ProSEDS mission, listed in Table 7 (Annex 1), was supposed to launch an electrodynamic tether system, with 15 km of length, in which 10 km would be of insulated material, and the remaining would be conductor. The mission was cancelled because of the possibility to collide with the ISS. Collisions problems between tethers in de-orbiting missions are also referred by [7], noting that if 40 de-orbits via TSS happens in a year, it means that only 4 tethers are in the space at a certain time, which reduce the probability of collisions events. The review article [7] does an exhaustive study of tethers.

Several authors study attitude dynamics of TSS in different configurations. Two-body and three-body systems have been mostly studied, but even tethered satellite constellations have been analyzed. In [24] the dynamics of three-body TSS is examined, with the *cm* following a circular orbit. A similar geometrical draw of the system is retracted in Chapter 3. In the referred article, a constant tether length constraint is also considered and equilibrium configurations are presented, as seen in Figure 2.5.2. Numerical results are given for several tether parameters, including tether lengths, tether speeds variations, and tether tensions. A dual spacecraft configuration that uses tethers for body connection [25], is suggested, with some interesting arrangements: parallel, parachute and single tether-connected body geometries.

In [26] and [27], A. Guerman considers the general problem of steady-state motions of a tethered satellite system in a circular orbit. All in-plane equilibrium configurations for arbitrary satellite masses and the tether lengths are found analytically in [26]. In [27] all possible spatial equilibrium configurations are described, and several classes of three-dimensional tethered formations are found. Tetrahedral formations which are of special interest for space applications are examined in detail, including the stability analysis, by Guerman et al. in [28].

In [29], S. Yu presents a control law for the tether length (known as range rate control algorithm) and demonstrates the equilibrium state as a function of the rotation angle. A circular and an orbital case are analyzed. Perturbations of motion are considered, namely the gravitational, centrifugal, and Coriolis forces.

A. K. Misra [30] addresses the nonlinear motions of a three dimensional TSS. Hamiltonian formulation is used and Poincaré sections for planar (pitch) and coupled motion (pitch and roll) are shown [31]. Non-chaotic motion is found for pitch and roll angles inferior or equal to 26°, as the Lyapunov exponent approaches zero over time. The same article evaluates the effect of aerodynamic and electrodynamic forces as well as the lifetime prediction and orbital decay of the system.

A. Burov, I. Kosenko, and A. Guerman in [32] study the dynamics of a moon-anchored tether with a material point at its end for variable tether length. The two-dimensional problem is addressed as a simple model for the lunar elevator. In this problem, some particular solutions of the motion equation are derived, choosing a specific control law for the tether length and finding radial and oblique configurations for the system geometry, while defining regions of stability and instability for each case.

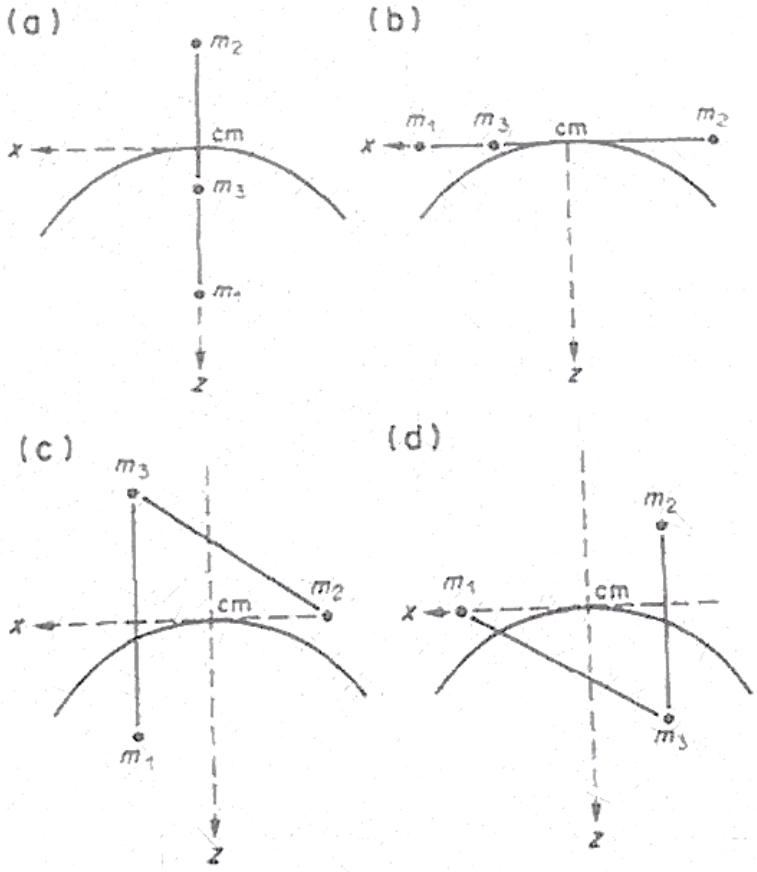

Figure 2.5.2 Equilibrium configurations

In [33] (W. Zhang and M. Yao), the periodic solution and stability of a tethered satellite system are found. As the authors refer, and should be cited, “the total mechanical energy of the system is minimum when the motion coincides with the periodic solution”, implying that “the periodic solution is the minimum energy solution, and the periodic solution in an elliptic orbit has the same significance as the equilibrium state in a circular orbit from the mechanical point of view”. The search of periodic solutions provides information about the equilibrium and/or critical solutions.

In [34], dynamics of a dumbbell composed by two masses connected by a lightweight tether is analyzed in an elliptic orbit. The system can serve as a simplified model for a two-body tether connected spacecraft. The article focuses on a specific tether control law to guarantee a uniform rotation of the system in terms of the true anomaly. Study of chaotic and regular motion, as well as stability analysis are also done.

Chapter 3 – Mathematical model of a two body tethered satellite system (TSS)

3.1 Introduction

The main objective of this dissertation is to analyze dynamics of a two bodies TSS in an elliptical orbit. The image of such system can be seen in Figure 3.1.1. The model is a dumbbell-like system, with the two mass points connected with a rigid and massless tether. The system's center of mass moves along an elliptic Keplerian orbit fixed in an inertial reference frame EXY connected to the center of the Earth (Fig. 3.1.2).

Figure 3.1.1 Satellite system connected with a tether

For the following analysis, each satellite is considered as a mass point and the tether is assumed to be massless. In this model, the positions of the two mass points are described with respect to the position of the center of mass of the system (C). The angles υ and φ represent the true anomaly and the angle between the tether and the position vector of the cm EC, respectively, ρ is the distance from E to C, $l_1$and l_2 are the distances between the mass points m_1 and m_2 and C, respectively, the length of the tether is $l = l_1 + l_2$.

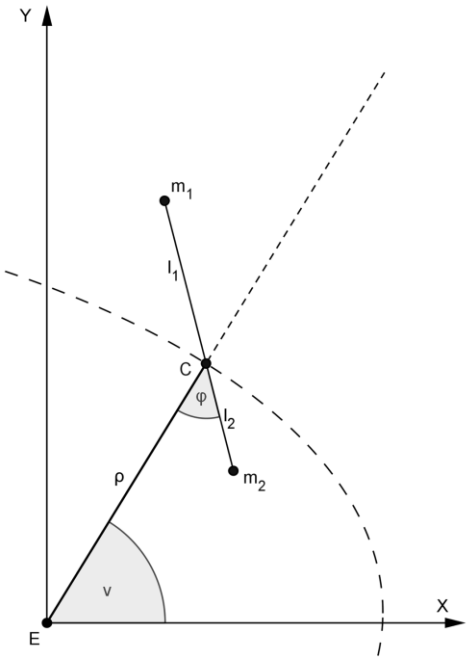

Figure 3.1.2 Dumbbell-like system composed by a massless tether and two mass points.

3.2 Mathematical model

The mathematical model is obtained in the following steps [34]:

i. Position of the center of mass based on $l_1$and l_2 lengths;

ii. ρ, $\mathrm{r}_1$and r_2 description based on Keplerian orbits;

iii. Potential Energy;

iv. Kinetic Energy;

v. Lagrange Equations of Motion.

3.2.1 Center of mass

Remembering the definition of the center of mass, and considering

$$l = l_1 + l_2 \quad (1)$$

(Figure 3.1.2), one obtains:

$$m_1 * l_1 = m_2 * l_2 \quad (2)$$

Substituting Equation (1) in to Equation (2), arrives at:

$$l_1 = \frac{m_2 * l}{m_1 + m_2} \quad (3)$$

$$l_2 = \frac{m_1 * l}{m_1 + m_2} \quad (4)$$

With these equations, the length of each part of the tether is known in function of the masses m_1, m_2, and the total tether length l.

3.2.2 Positions of the system

As stated before (see Section 2.4), we consider here that the size of the system is small compared to the orbit dimensions, which allows the motion to be described by the Keplerian formula:

$$\rho = \frac{p}{1 + e * cos(\nu)} \quad (5)$$

with

- p as the focal parameter,
- e as the eccentricity,
- ν as the true anomaly

The meaning of the above parameters can be seen in [35] (Chapter 2). The system coordinates are:

$$x_0 = \rho * cos(\nu) \qquad y_0 = \rho * sin(\nu)$$
$$x_1 = x_0 + l_1 * cos(\nu + \varphi) \qquad y_1 = y_0 + l_2 * sin(\nu + \varphi) \quad (6)$$

$$x_2 = x_0 - l_2 * cos(v + \varphi) \qquad y_2 = y_0 - l_2 * sin(v + \varphi)$$

where

- x_0 and y_0 are the components of the position vector of the center of mass, $\overrightarrow{r_0}$
- x_1 and y_1 are the components of the position vector of the point mass 1, $\overrightarrow{r_1}$
- x_2 and y_2 are the components of the position vector of the point mass 2, $\overrightarrow{r_2}$

$$\begin{cases} \overrightarrow{r_0} = (x_0, y_0) \\ \overrightarrow{r_1} = (x_1, y_1) \\ \overrightarrow{r_2} = (x_2, y_2) \end{cases} \quad (7)$$

3.2.3 Potential energy of the system

The potential energy of the system can be obtained using the following expression:

$$V = -\sum_{i=1}^{n} \frac{\mu_0 * m_i}{\|\overrightarrow{r_i}\|} \quad (8)$$

where:

- *n* represents the number of total mass points of the system
- m_i represents the mass of the point
- $\overrightarrow{r_i}$ represents the position vector of the point mass with respect to the Earth's center
- $\mu_0 = G * M$
- G represents the universal gravitational constant
- M is the mass of the Earth

For the problem in study, Equation (8) reads

$$V = -\frac{\mu_0 * m_1}{\|\overrightarrow{r_1}\|} - \frac{\mu_0 * m_2}{\|\overrightarrow{r_2}\|} \quad (9)$$

Introducing two new variables μ and m:

$$\mu = \frac{m_1}{m} \tag{10}$$

$$m = m_1 + m_2 \tag{11}$$

Equation (9) becomes:

$$V = -\mu_0 * m\left(\frac{\mu}{\|\vec{r_1}\|} + \frac{1-\mu}{\|\vec{r_2}\|}\right) \tag{12}$$

or

$$V = -\mu_0 * m\left(\frac{\mu}{\sqrt{{x_1}^2 + {y_1}^2}} + \frac{1-\mu}{\sqrt{{x_2}^2 + {y_2}^2}}\right) \tag{13}$$

Introducing a new variable λ,:

$$\lambda = \frac{l}{p} \tag{14}$$

and assuming $\lambda \ll 1$, i.e., the tether length is much smaller than the focal parameter p, one can write the Taylor series expansion of 2nd order for V as:

$$V = -\frac{m\,\mu 0\,(1 + e * cos(v))}{p} + \frac{m\,(-1+\mu)\,\mu\,\mu 0\,(1 + e * cos(v))^3\,(1 + 3 * cos(2\,\varphi))\lambda^2}{4p} \tag{15}$$

Here we omit the terms of the third and higher orders with respect to λ.

3.2.4 Kinetic energy of the system

The kinetic energy of the system can be obtained using the following equation:

$$T = \sum_{i=1}^{n} \frac{m_i * {v_i}^2}{2} \tag{16}$$

where

- n represents the number of total mass points of the system
- m_i represents the mass of the point *i*

- $\vec{v_i}$ represents the vector velocity of the point mass *i*

Since

$$v_i = \|\dot{\vec{r_i}}\| \tag{17}$$

while denoting

$$\left(\dot{}\right) = \frac{d}{dt} \tag{18}$$

one obtains

$$v_i = \sqrt{\dot{x_i}^2 + \dot{y_i}^2} \tag{19}$$

Returning to Equation (16),

$$T = \frac{m_1 * \left(\dot{x_i}^2 + \dot{y_i}^2\right)}{2} + \frac{m_2 * \left(\dot{x_2}^2 + \dot{y_2}^2\right)}{2} \tag{20}$$

$$T = \frac{1}{4} m \left[\frac{2p^2(1 + e^2 + 2e\cos\nu)\dot{\nu}^2}{(1 + e\cos\nu)^4} - 2(-1 + \mu)\mu(\dot{l}^2 + l^2(\dot{\nu} + \dot{\varphi})^2)\right] \tag{21}$$

3.2.5 The Lagrangian equations of motion

The Lagrangian equations of motion are known as *differential equations of system motion in generalized coordinates*. In fact, the Lagrangian equations provide a simple way to obtain the system positions in function of time [36, 37]. It was decided to choose the Lagrangian formulation because it allows us to define the global positions of the system through potential and kinetic energy and in function of generalized coordinates, unlike the needs to define all the forces and coordinates involved, as in Newtonian formulation.

The Lagrangian equation is:

$$\frac{d}{dt}\left(\frac{\partial L}{\partial \dot{q}_j}\right) - \frac{\partial L}{\partial q_j} = Q_j \tag{22}$$

where $L = T - V$, q_j is the generalized coordinate and Q_j is the generalized force actuating in the system.

For the conservative case one has:

$$\frac{d}{dt}\left(\frac{\partial L}{\partial \dot{q}_j}\right) - \frac{\partial L}{\partial q_j} = 0 \tag{23}$$

For the following analysis, the generalized coordinates are φ and l and the system is only under the gravitational forces. Two equations can be obtained:

$$\frac{d}{dt}\left(\frac{\partial L}{\partial \dot{\varphi}}\right) - \frac{\partial L}{\partial \varphi} = 0 \qquad \frac{d}{dt}\left(\frac{\partial L}{\partial \dot{l}}\right) - \frac{\partial L}{\partial l} = 0 \tag{24}$$

Defining φ or l as a function of time allows one to find the remaining parameter as a control for system, as can be seen in Chapter 4. It has been chosen to define the desirable law for re-orientation $\varphi = \varphi(t)$ and obtain the respective control law for the tether length $l = l(t)$. Therefore, the first equation in Equations (24) should be studied. After some simplifications, it becomes:

$$l\left(3\,\mu 0\; sin(2\varphi)(e\cos(\nu)+1)^3 + 2p^3(\ddot{\nu}+\ddot{\varphi})\right) + 4p^3\dot{l}(\dot{\nu}+\dot{\varphi}) = 0 \tag{25}$$

All these variables are time-related. For a more advantageous formulation, consider new independent variable, the *true anomaly* ν. A new change of variables and definitions is introduced:

$$(\,)' = \frac{d}{d\nu} \tag{26}$$

$$\dot{\nu} = \omega_0(1 + e\; cos\; \nu)^2 \tag{27}$$

with

$$\omega_0{}^2 = \frac{\mu_0}{p^3} \tag{28}$$

The chain rule applies here, where

$$(f\; o\; g)'(c) = (f' o\; g)(c) * g'(c) \tag{29}$$

and $\ddot{\nu}$ becomes

$$\ddot{\nu} = -\frac{2e\;\mu 0\; sin(\nu)(e\; cos\; \nu + 1)^3}{p^3} \tag{30}$$

For the other parameters, the same change occurs, although the result is suppressed:

$$\dot{\varphi} = \varphi' * \dot{\nu} \tag{31}$$

$$\ddot{\varphi} = \varphi'' * \dot{\nu} * \dot{\nu} + \varphi' * \ddot{\nu} \tag{32}$$

$$\dot{l} = l' * \dot{\nu} \tag{33}$$

$$\ddot{l} = l'' * \dot{\nu} * \dot{\nu} + l' * \ddot{\nu} \tag{34}$$

Substituting all these variables, Equation (25) becomes:

$$\begin{aligned}(e\,cos(\nu) + 1)\Big(&4l'\,(\varphi' + 1)(e\,cos(\nu) + 1) \\ &+ l\big(2\varphi''(e\,co\,s\,\nu + 1) - 4e\,sin(\nu)\varphi' - 4e\,sin(\nu) + 3\,sin(2\varphi)\big)\Big) = 0\end{aligned} \tag{35}$$

which can be rearranged as

$$(1 + e\,cos\,\nu) * \varphi'' + 2\left[\frac{l'}{l} * (1 + e\,cos\,\nu) - e * sin\,\nu\right](1 + \varphi') + 3\,cos\varphi\,sin\varphi = 0 \tag{36}$$

a well-known equation [34] [38]. Note that this equation does not depend on the mass of the system.

Chapter 4- Control laws

At this stage, the Lagrangian equations of motion have been derived. Now we can choose the desired variation of the system's attitude $\varphi = \varphi(\nu)$ (the programmed re-orientation of the tether) and obtain the equation for the respective control law for the tether length $l = l(\nu)$.

Two modes of the behavior of φ are presented: the uniform rotations and fixed orientation with respect to the local vertical. Each case is analyzed independently.

4.1 Uniform rotations

For uniform rotations, the control law can assume the following form [34] [39]:

$$\varphi = \omega\, \nu + \varphi_0 \tag{37}$$

This relation means that the actual angle of rotation depends on the initial condition φ_0, the variation of ν and a constant ω (angular velocity).

Equation (36) can be rewritten:

$$2\left[\frac{l'}{l}(1 + e\cos(\nu)) - e\sin(\nu)\right](1 + \omega) - 3\cos(\omega\,\nu + \varphi_0)\sin(\omega\,\nu + \varphi_0) = 0 \tag{38}$$

Resolving this equation for $\frac{l'}{l}$, yields

$$\frac{l'}{l} = \frac{2e\sin\nu + 2e\,\omega\sin\nu - 3\cos(\omega\nu + \varphi_0)\sin(\omega\nu + \varphi_0)}{2(1+\omega)(1 + e\cos\nu)} \tag{39}$$

which is equivalent to

$$\frac{l'}{l} = \frac{e\,sin\,\nu}{1 + e\,cos\,\nu} - \frac{3\,sin\,(2(\omega\nu + \varphi_0))}{4(1+\omega)(1 + e\,cos\,\nu)} \tag{40}$$

4.1.1 Tether behavior

Equation (40) allows one to obtain the tether length l as a function of ν. However, in the general case, analytical integration of (40) is not possible. For some values of ω the control law can be obtained in the close form; for other values of angular velocity ω the integration has to be performed numerically.

Here, some results are presented assuming that $\varphi_0 = 0$.

Figure 4.1.1.1 Tether logarithmic ratio for different eccentricities and $\omega = 0$

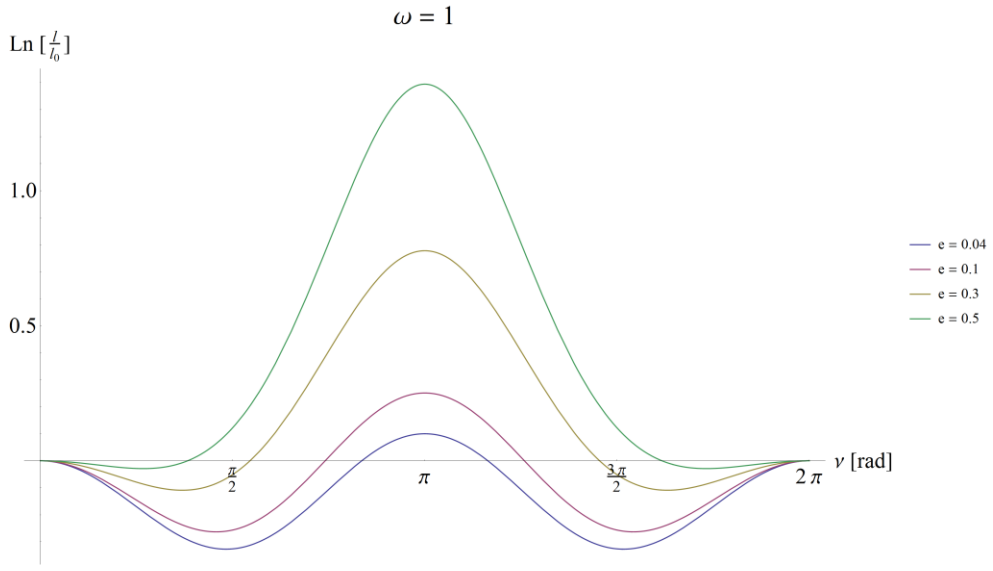

Figure 4.1.1.2 Tether logarithmic ratio for different eccentricities and $\omega = 1$

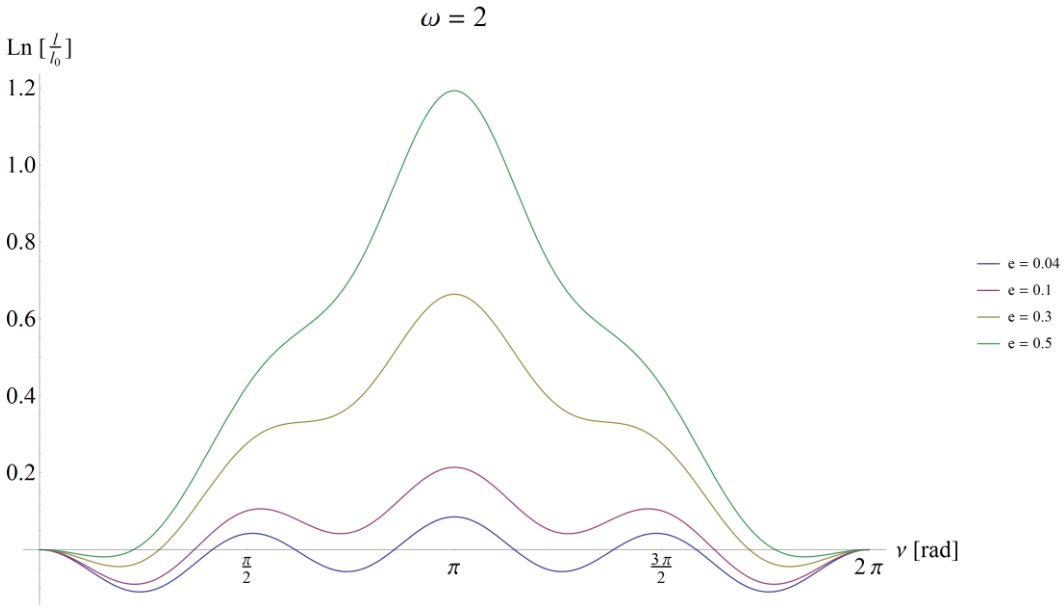

Figure 4.1.1.3 Tether logarithmic ratio for different eccentricities and $\omega = 2$

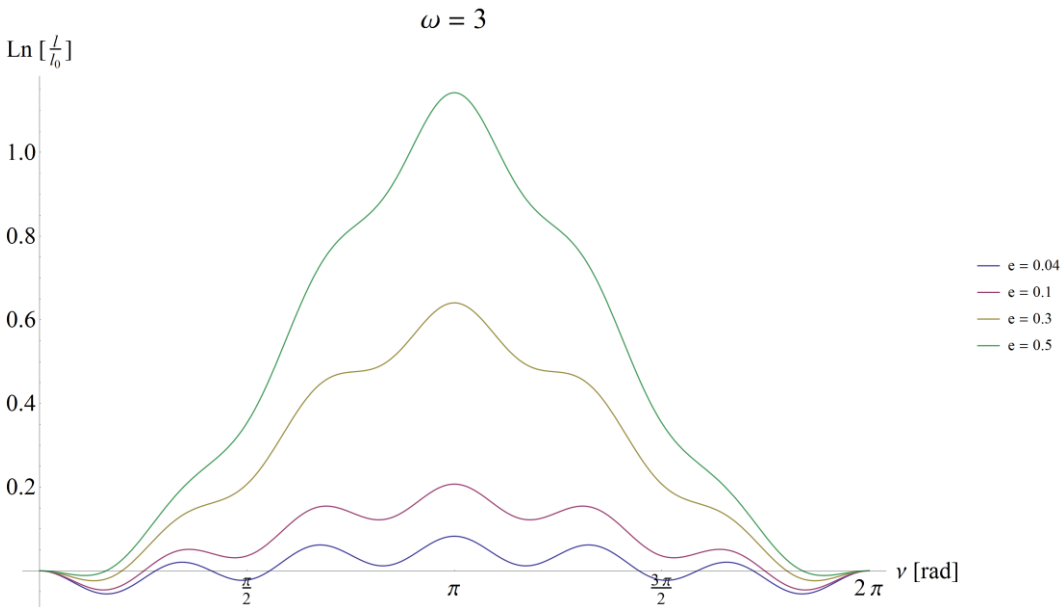

Figure 4.1.1.4 Tether logarithmic ratio for different eccentricities and $\omega = 3$

It is interesting to note that all the tether variations for those ω seem to be periodic. One can see that with increase of ω, the logarithmic curves have more oscillations, those being more noticable for small values of eccentricity. Inverse rotations ($\omega < 0$) are similar to those

presented (see Annex 2). For fractional values of ω, the tether may not assume a 2π periodic behavior.

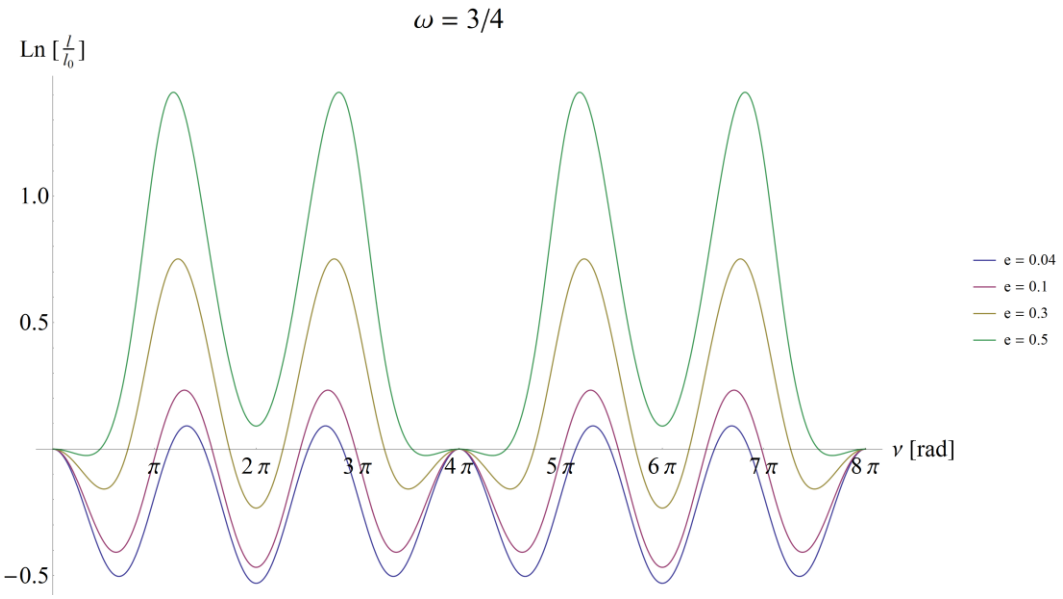

Figure 4.1.1.5 Tether logarithmic ratio for different eccentricities and $\omega = 3/4$

Also, as can be seen from Equation (38), for $\omega = -1$ the solutions do not exist.

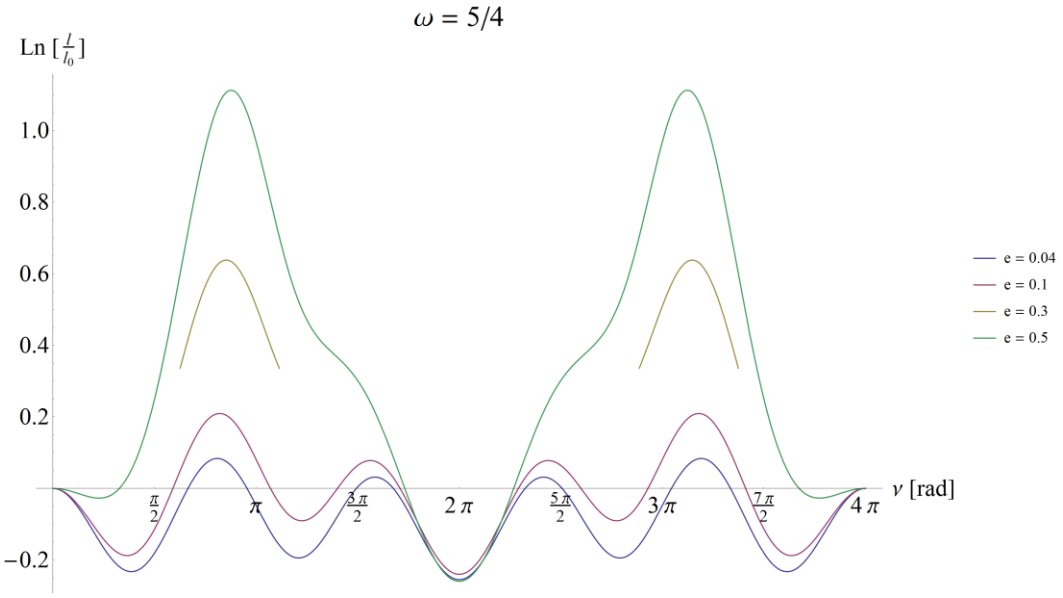

Figure 4.1.1.6 Tether logarithmic ratio for different eccentricities and $\omega = 5/4$

For more simulations, see Annex 2.

Although an analytical integration of Equation (40) is not possible, an approximation has been made to obtain a general formulation of the tether length for each ν. The results use the Taylor series of the 4th order and are presented below.

The approximation of the right-hand term of Equation **(40)** is:

$$
\begin{aligned}
& e^4\left(-\frac{3\cos^4(\nu)\sin(2\nu\omega)}{4(\omega+1)}-\sin(\nu)\cos^3(\nu)\right) \\
& \quad + e^3\left(\frac{3\cos^3(\nu)\sin(2\nu\omega)}{4(\omega+1)}+\sin(\nu)\cos^2(\nu)\right) \\
& \quad + e^2\left(-\frac{3\cos^2(\nu)\sin(2\nu\omega)}{4(\omega+1)}-\sin(\nu)\cos(\nu)\right) \\
& \quad + e\left(\frac{3\cos(\nu)\sin(2\nu\omega)}{4(\omega+1)}+\sin(\nu)\right)-\frac{3\sin(2\nu\omega)}{4(\omega+1)}
\end{aligned}
\qquad (41)
$$

considering $e \ll 1$. This expression allows integration, though the results are quite cumbersome and are omitted here. Some results are plotted below.

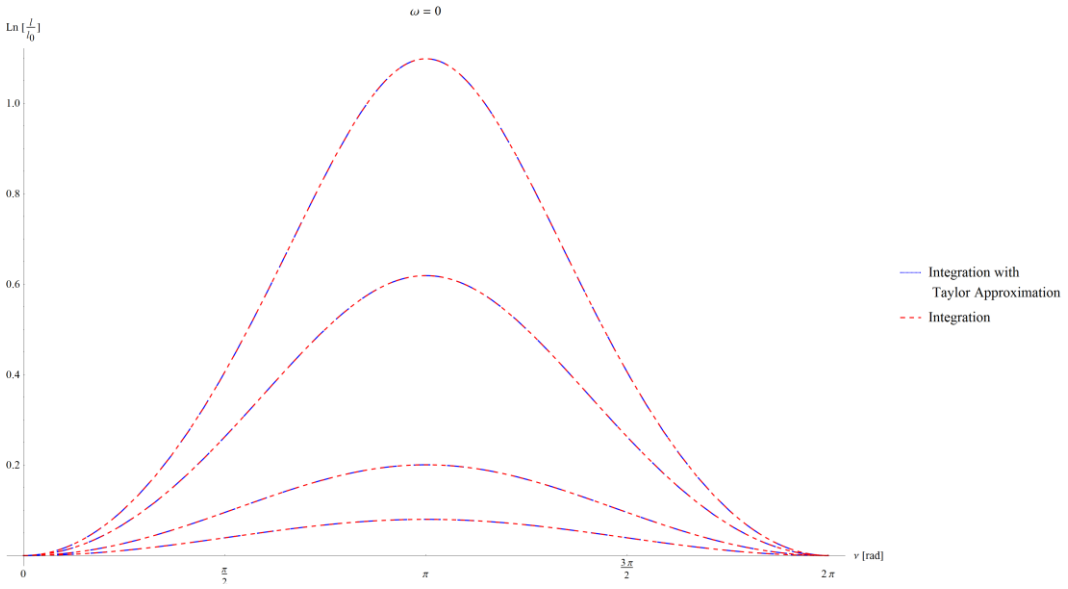

Figure 4.1.1.7 Tether logarithmic ratio approximation comparison and $\omega = 0$

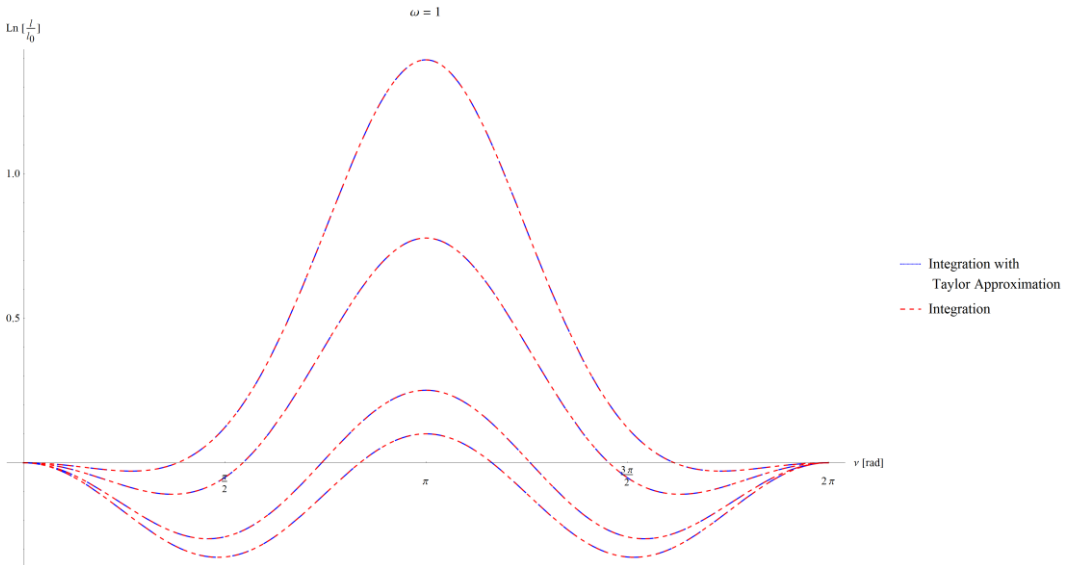

Figure 4.1.1.8 Tether logarithmic ratio approximation comparison and $\omega = 1$

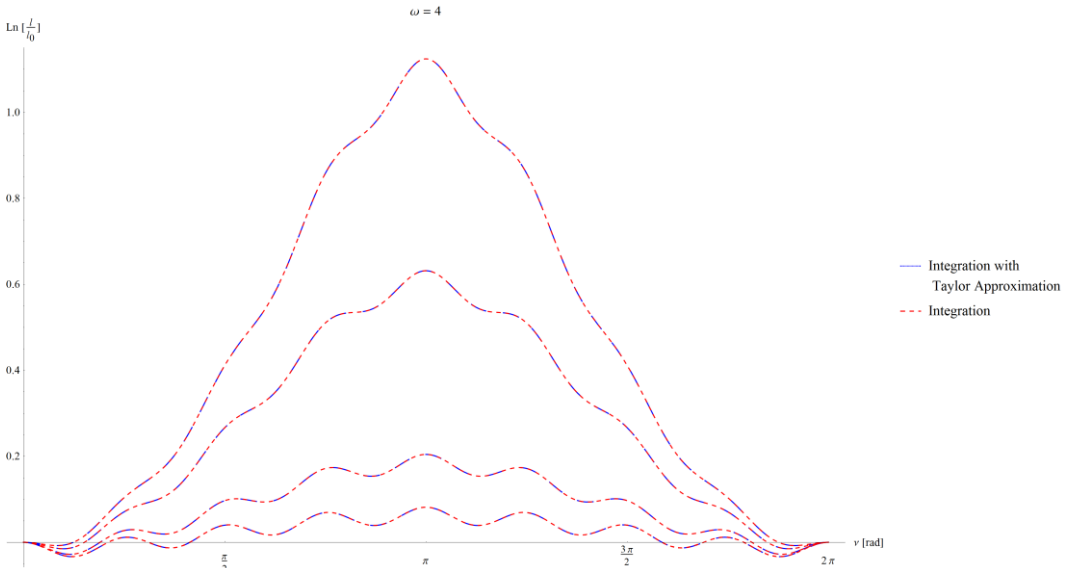

Figure 4.1.1.9 Tether logarithmic ratio approximation comparison and $\omega = 4$

The simulations above are made for $e = \{0.04\,, 0.1\,, 0.3, 0.5\}$. Note the similarity between the direct integration and the use of the approximation. Even for the fractional values of the angular velocity the approximation via Taylor series is very precise (see Figure 4.1.1.10).

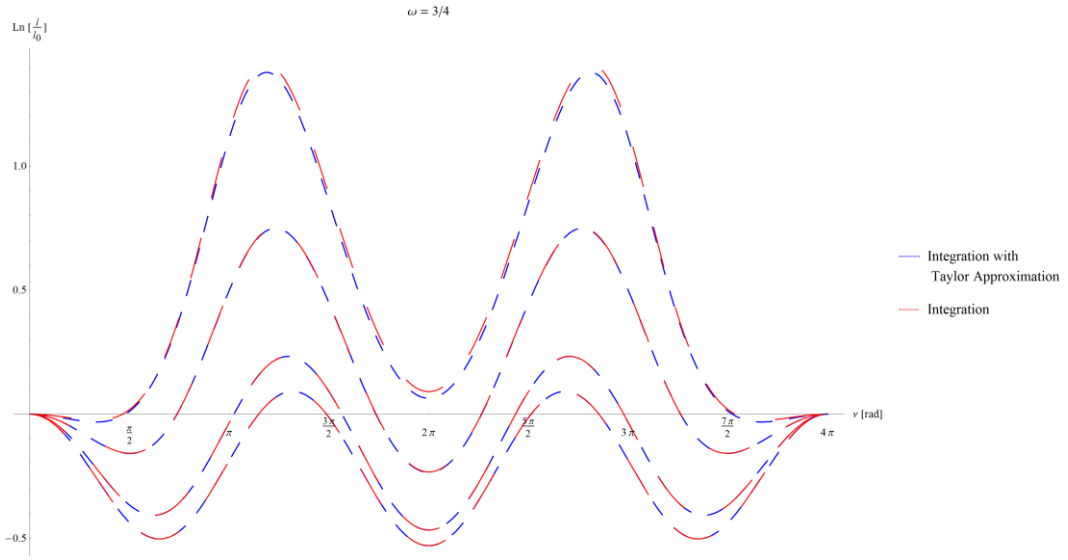

Figure 4.1.1.10 Tether logarithmic ratio approximation comparison and $\omega = 3/4$

The error of the approximation for $\omega = 0$ and for $e = 0.04$ and $e = 0.5$, can be seen in Figures 4.1.1.11 and 4.1.1.12.

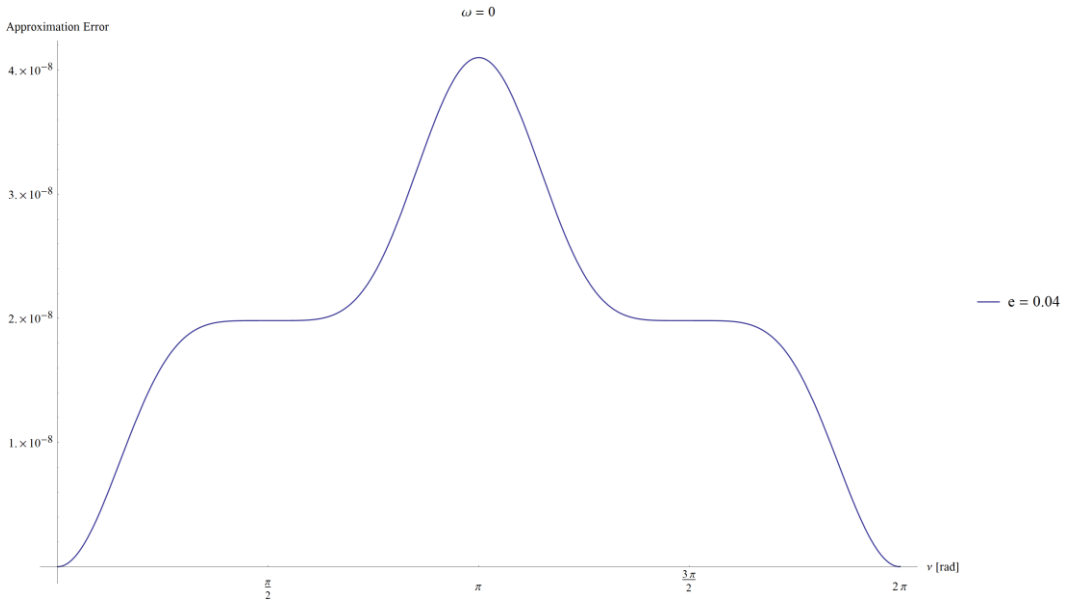

Figure 4.1.1.11 Approximation error for $e = 0.04$

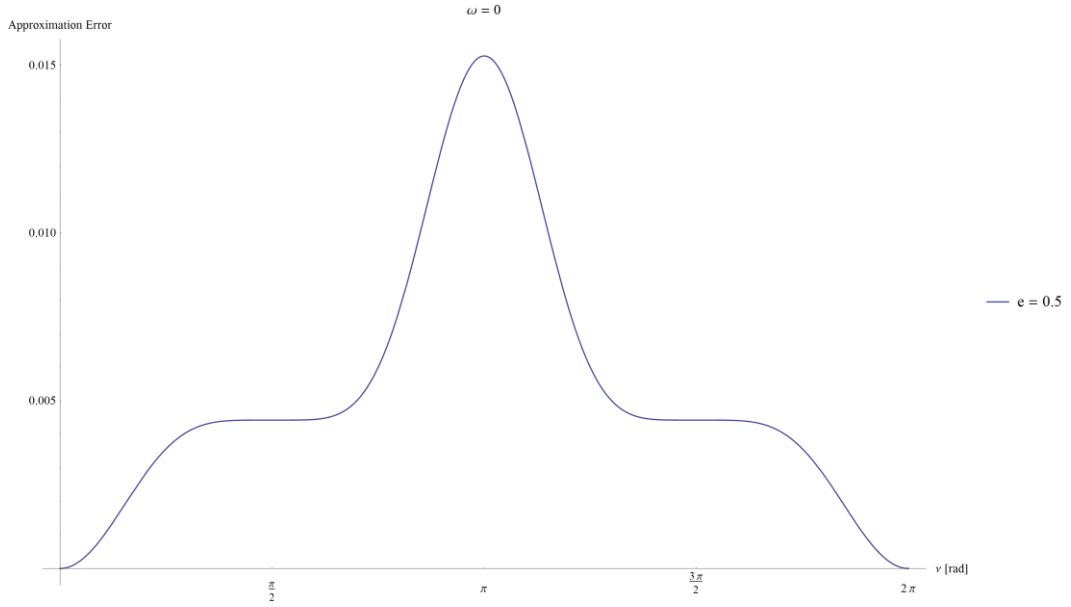

Figure 4.1.1.12 Approximation error for $e = 0.5$

The error increases as eccentricity also increases, since the approximation has been made considering $e \ll 1$. Simulations for other values of ω and e result in similar error ranges.

It should be noted this approximation introduces some new critical cases, where solutions don't exist. These critical cases correspond to $\omega = \left\{0; \frac{1}{2}; 1; \frac{3}{2}; 2; -\frac{1}{2}; -\frac{3}{2}; -2\right\}$, as indeterminations appear. Although some of the graphics using the approximation for those ω are presented in this document, the neighborhood was taken into account.

The contour plots can also be a good tool to illustrate the tether behavior as function of ω and e. At Figures 4.1.1.13 - 4.1.1.15 it is possible to see the logarithmic values of the tether ratio $\frac{l}{l_0}$ for some eccentricities (the color legend refers to those values):

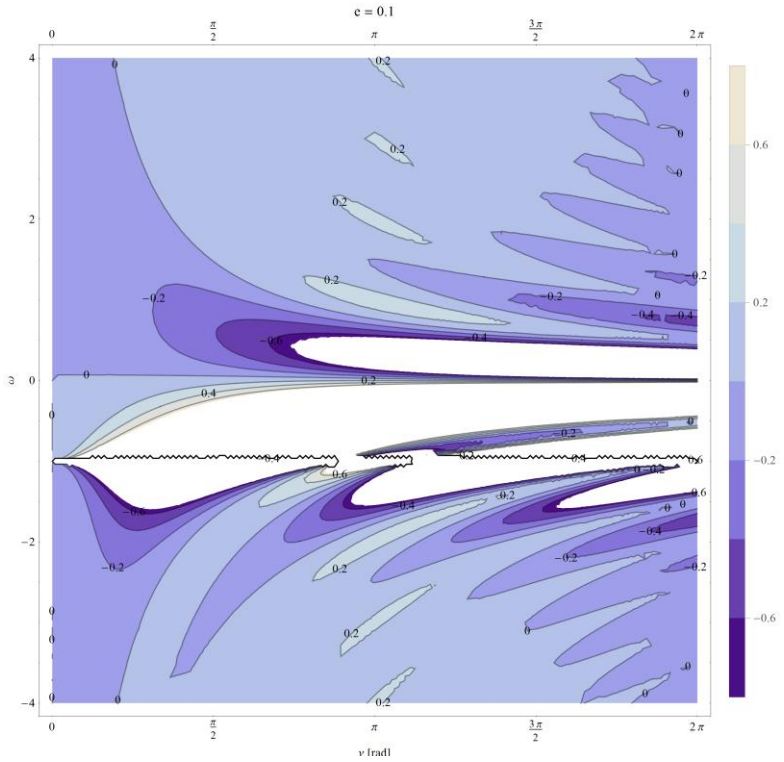

Figure 4.1.1.13 Tether logarithmic ratio - Contour Plot for $e = 0.1$

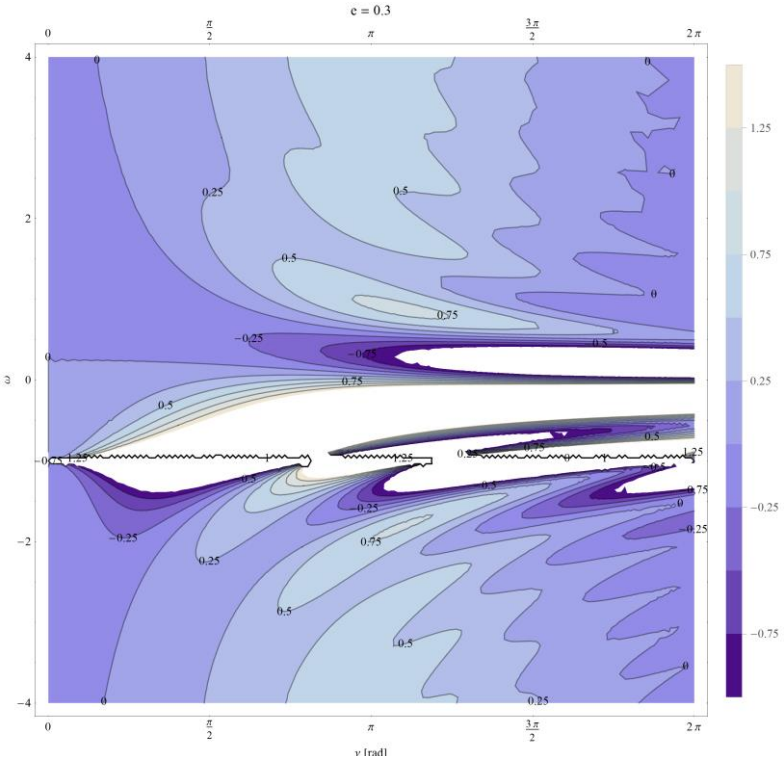

Figure 4.1.1.14 Tether logarithmic ratio - Contour Plot for $e = 0.3$

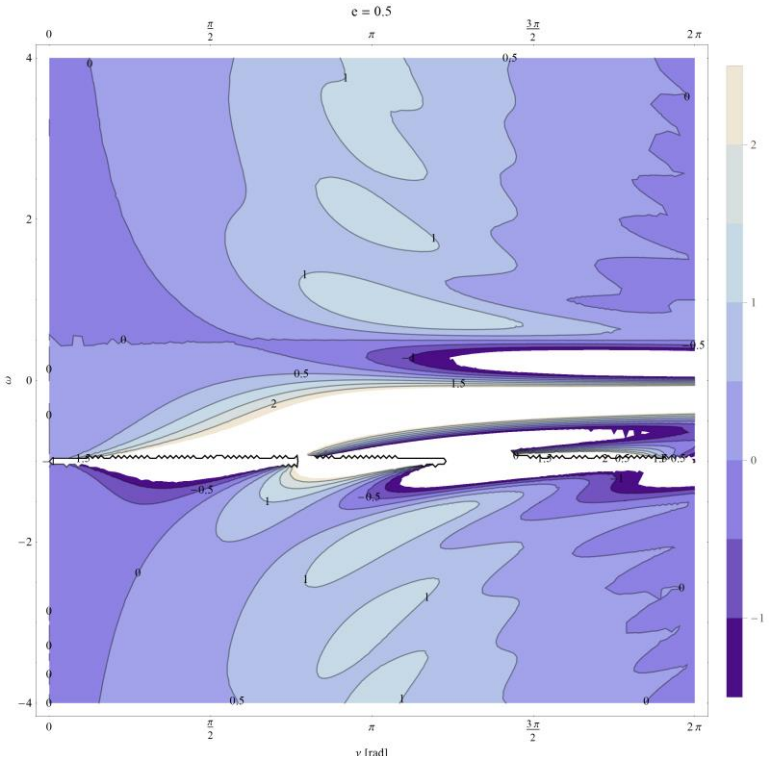

Figure 4.1.1.15 Tether logarithmic ratio - Contour Plot for $e = 0.5$

Those contours are obtained using the already described approximation. Note the similarity in white regions between the two graphics, as they represent the indeterminate cases from the approximation.

For periodicity analyzes (in terms of ν), the same plots are done, but for a larger range of the independent variable ν (Figures 4.1.1.16, 4.1.1.17 and 4.1.1.18).

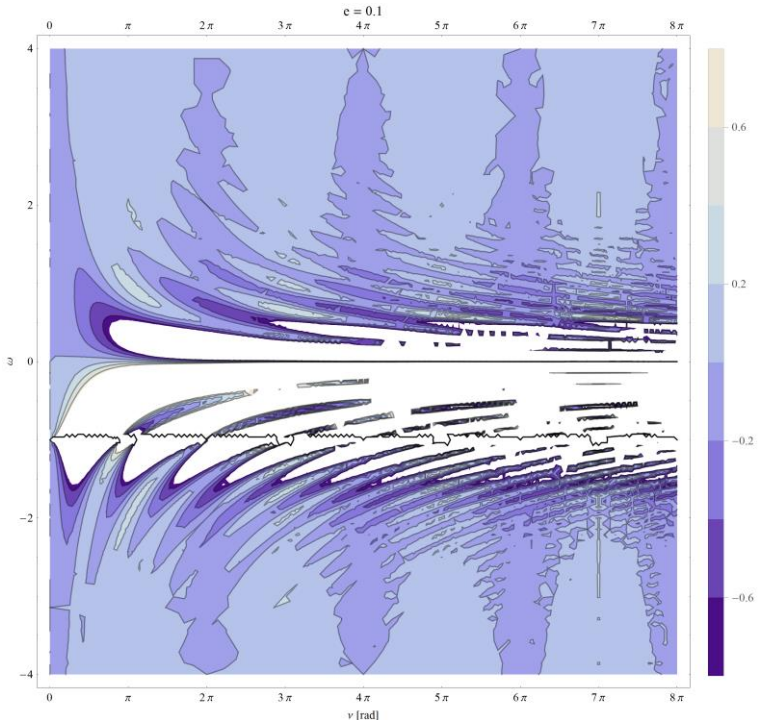

Figure 4.1.1.16 Tether logarithmic ratio - Contour Plot for $e = 0.1$ and periodic findings

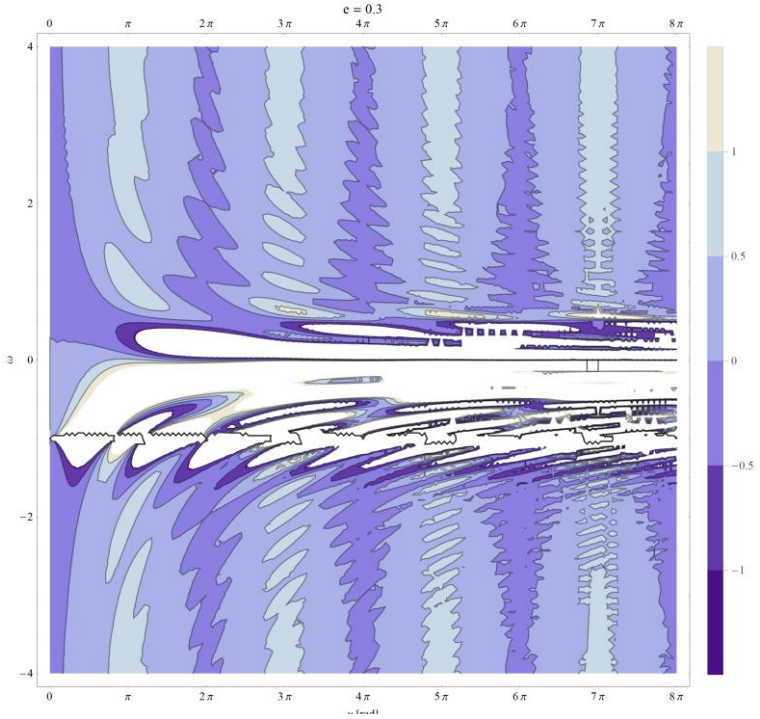

Figure 4.1.1.17 Tether logarithmic ratio - Contour Plot for $e = 0.3$ and periodic findings

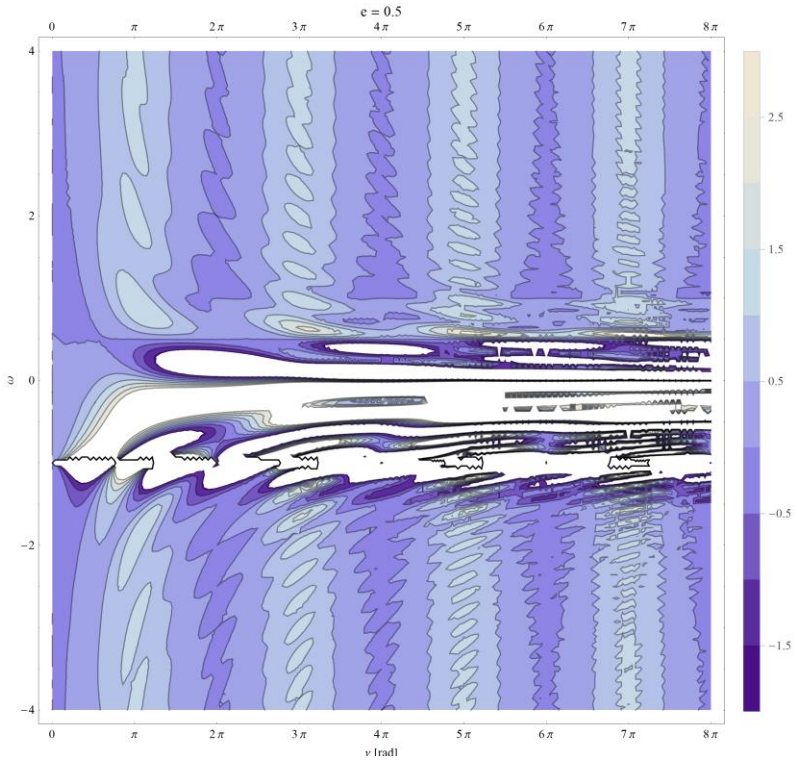

Figure 4.1.1.18 Tether logarithmic ratio - Contour Plot for $e = 0.5$ and periodic findings

As it can be seen, in the last three figures (Figures 4.1.1.16, 4.1.1.17 and 4.1.1.18), none shown a fully-periodic behavior for the range of ω chosen. In fact, the integration of the Equation **(41)** leads to the appearance of non-periodic solutions; they can be seen in the mentioned figures.

4.2 Permanent orientation

In many cases (such as, e.g., for GPS data transmission), the satellite should keep its orientation with respect to the local vertical. As stated in Chapter 2, such orientation in a circular orbit can be kept via proper mass distribution of a satellite. However, in an elliptic orbit, the permanent orientation of the system with respect to the local vertical requires some sort of active control. Here we consider the possibility to control the orientation of two-body tethered system by changing the tether's length.

This control law can assume the following expression:

$$\varphi = \varphi_0 \qquad (42)$$

allowing to rewrite Equation (40) into

$$\frac{l'}{l} = \frac{e\ sin\ \nu}{1 + e\ cos\ \nu} - \frac{3\ sin\ (2\varphi_0)}{4(1 + e\ cos\ \nu)} \qquad (43)$$

4.2.1 Tether behavior

As before, the closed-form integration is also not possible. Therefore numerical integration has been performed for a number of values of φ_0, obtaining the control laws shown in Figures 4.2.1.1-4.2.1.4.

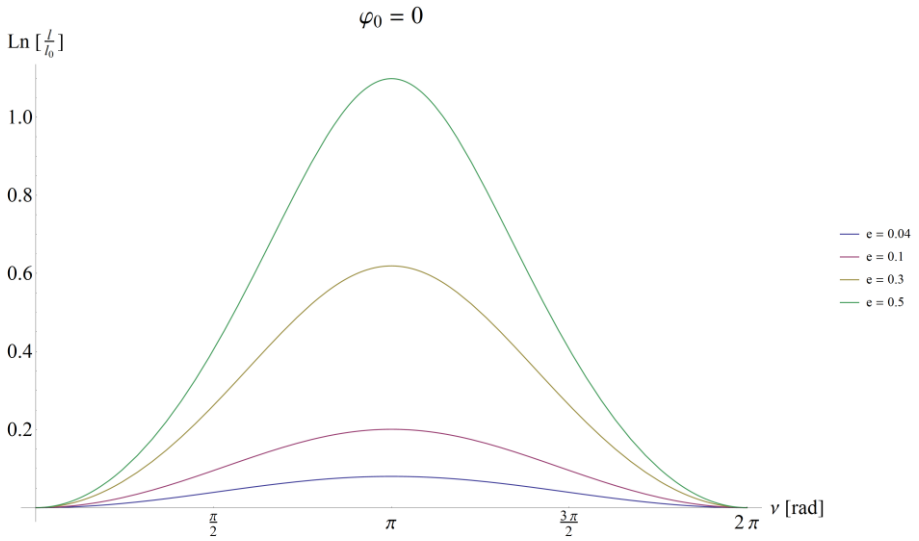

Figure 4.2.1.1 Tether logarithmic ratio for different eccentricities for $\varphi_0 = 0$

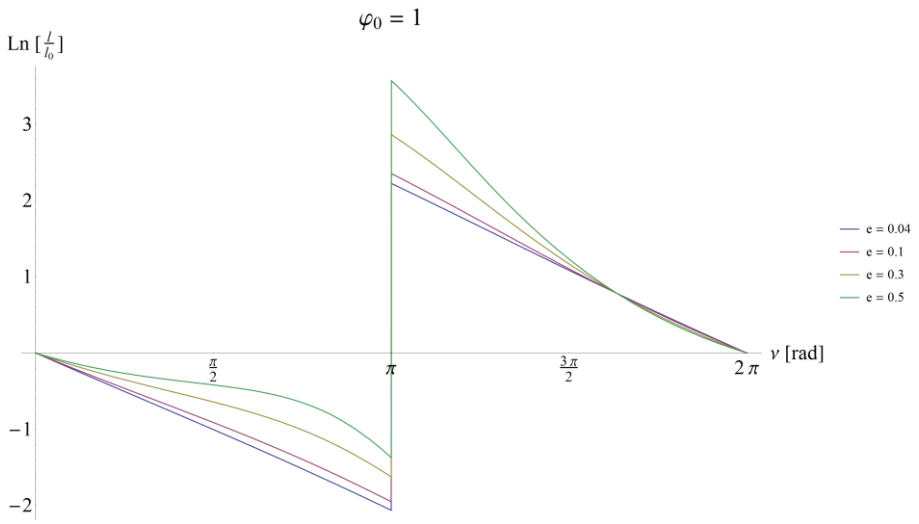

Figure 4.2.1.2 Tether logarithmic ratio for different eccentricities for $\varphi_0 = 1$

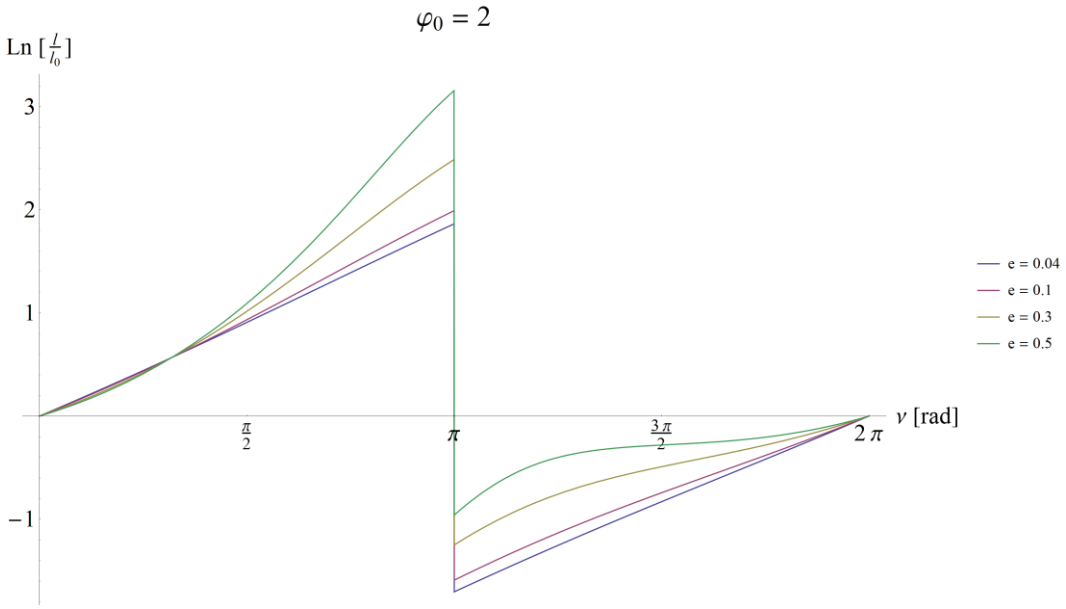

Figure 4.2.1.3 Tether logarithmic ratio for different eccentricities for $\varphi_0 = 2$

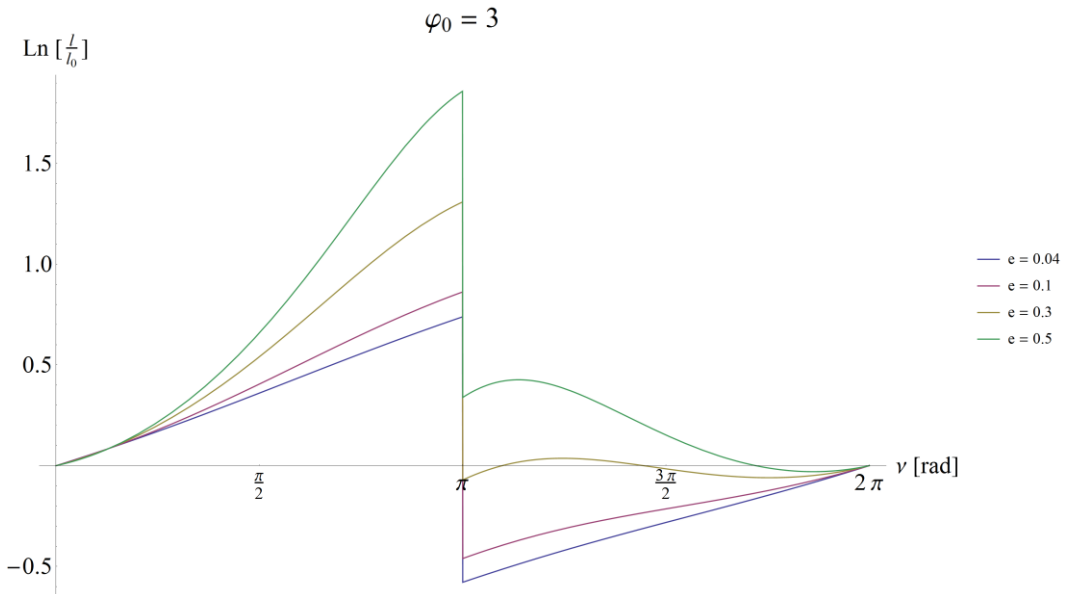

Figure 4.2.1.4 Tether logarithmic ratio for different eccentricities for $\varphi_0 = 3$

Further simulations are presented in Annex 2. Note the similarity of the first case, $\varphi_0 = 0$, with the linear case for $\omega = 0$, as it is an equivalent equation.

In the case of permanent orientation for values $\nu = k\,\pi$ (k as an even integer) the tether length should change its behavior discontinuously. In this case the implementation of the control along the whole orbit is impossible.

For an analytical solution, an approximation of 4th order using the Taylor series is also done allowing the integration of Equation (43). Some solutions are plotted in Figures 4.2.1.5 - 4.2.1.7.

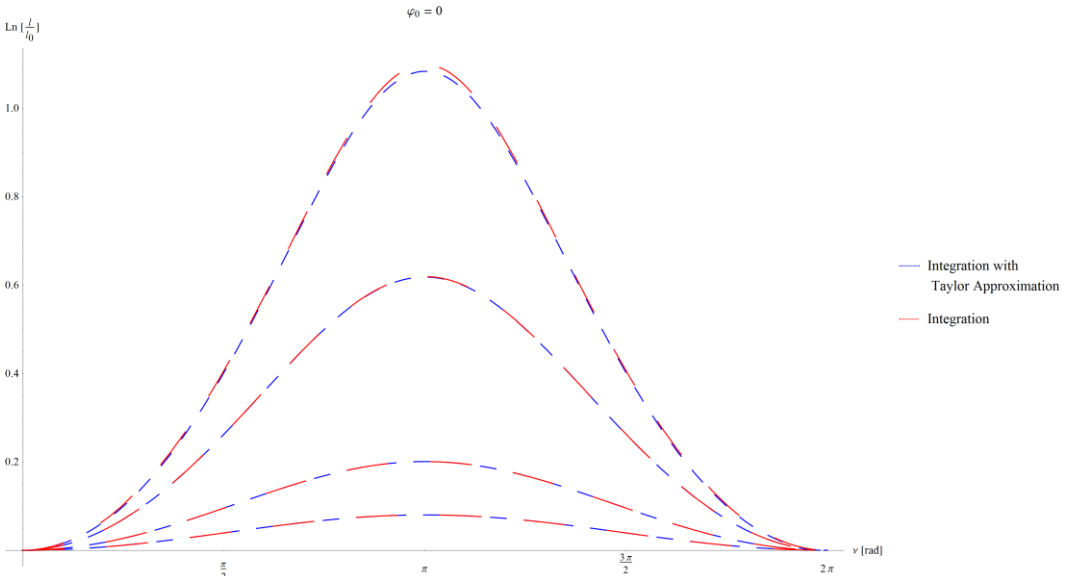

Figure 4.2.1.5 Tether logarithmic ratio approximation comparison with $\varphi_0 = 0$

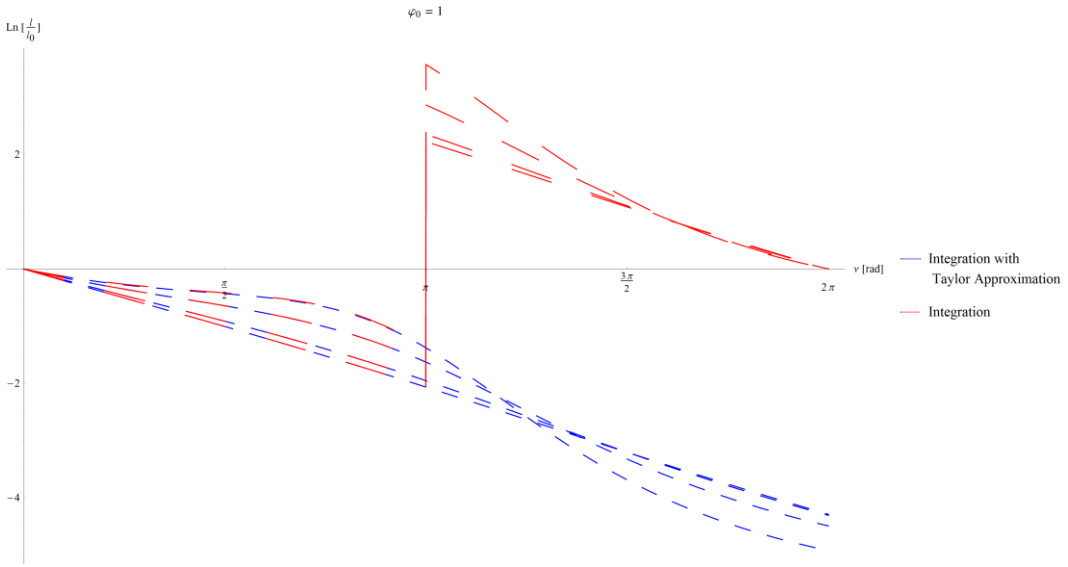

Figure 4.2.1.6 Tether logarithmic ratio approximation comparison with $\varphi_0 = 1$

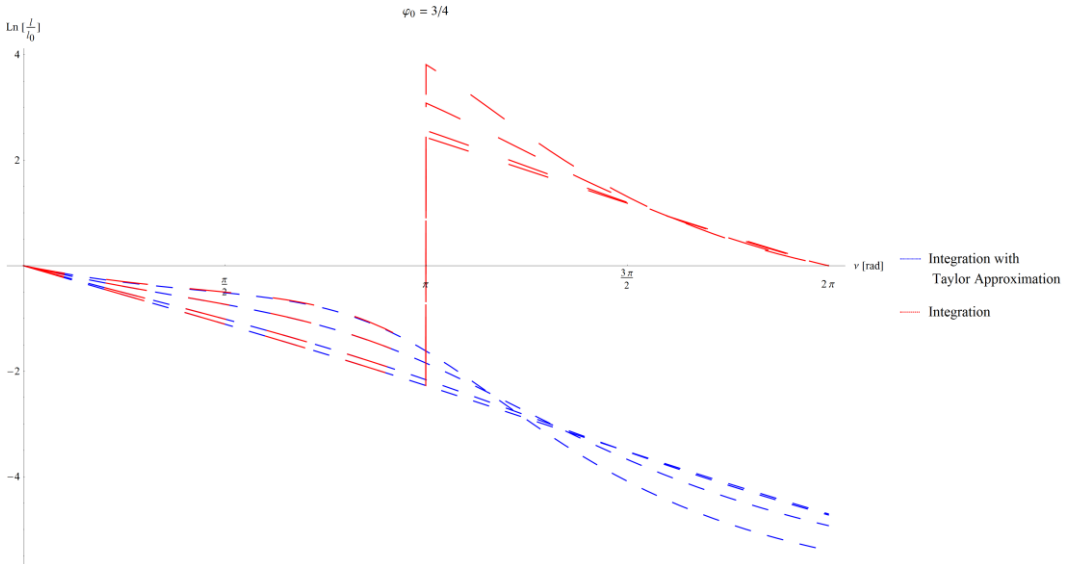

Figure 4.2.1.7 Tether logarithmic ratio approximation comparison with $\varphi_0 = 3/4$

As it can be seen in Figures 4.2.1.6 and 4.2.1.7, the approximation only works for [0,π], since the approximation can't accomplish the abrupt change at $\nu = \pi$. The associated error for $e = 0.04$ and $\varphi_0 = 1$ is shown in Figure 4.2.1.8. :

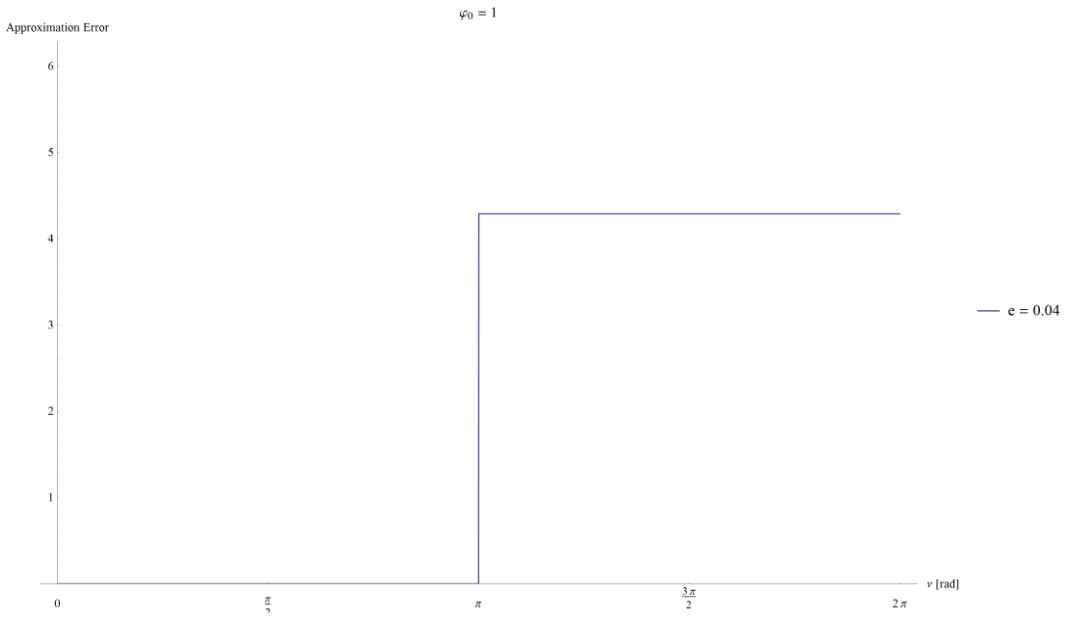

Figure 4.2.1.8 Approximation error for eccentricity = 0.04

The contours can also be seen in Figures 4.2.1.9, 4.2.1.10 and 4.2.1.11, respectively, for $e = 0.1$, $e = 0.3$ and $e = 0.5$.

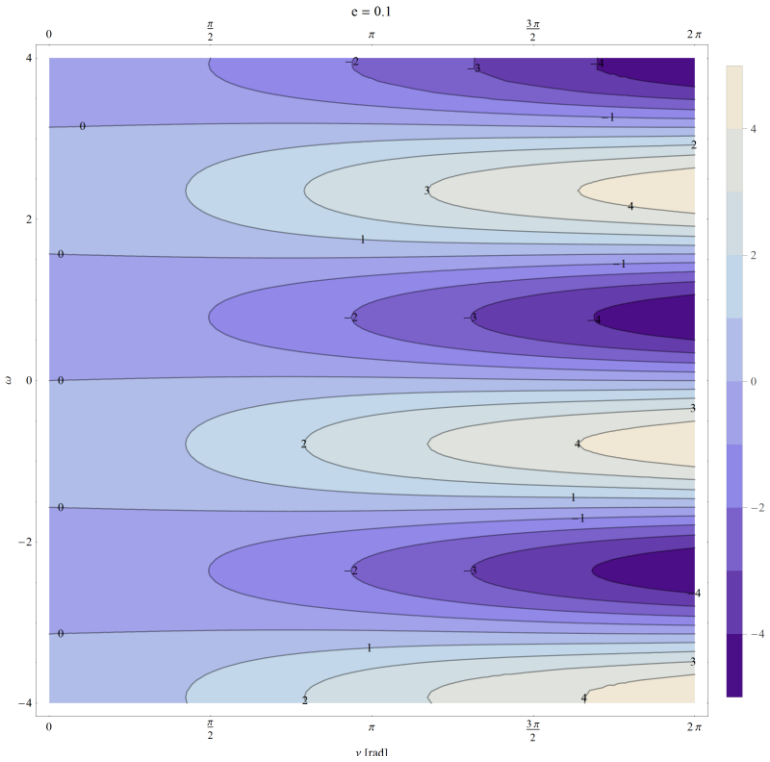

Figure 4.2.1.9 Tether logarithmic ratio - Contour Plot for $e = 0.1$

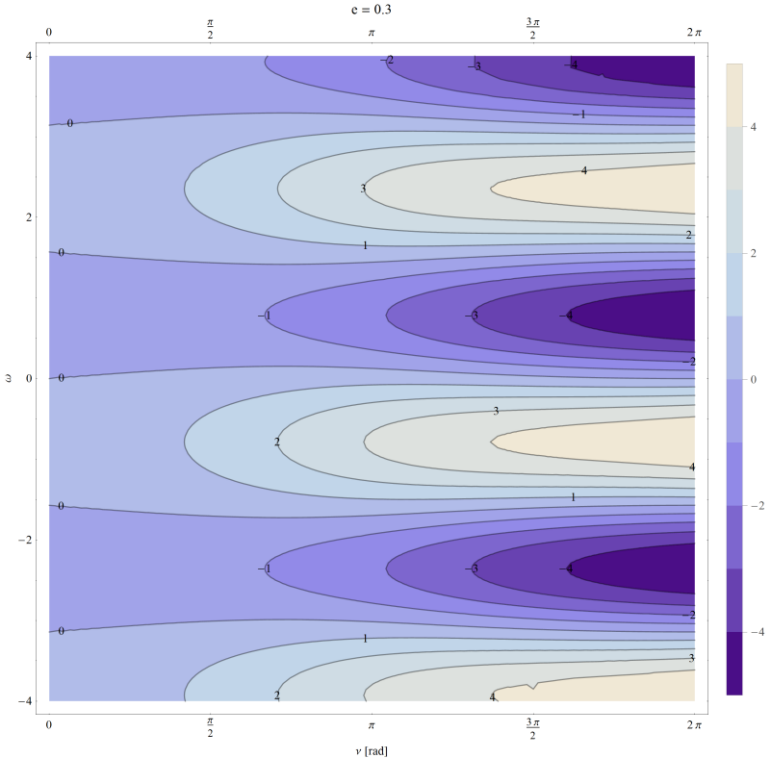

Figure 4.2.1.10 Tether logarithmic ratio - Contour Plot for $e = 0.3$

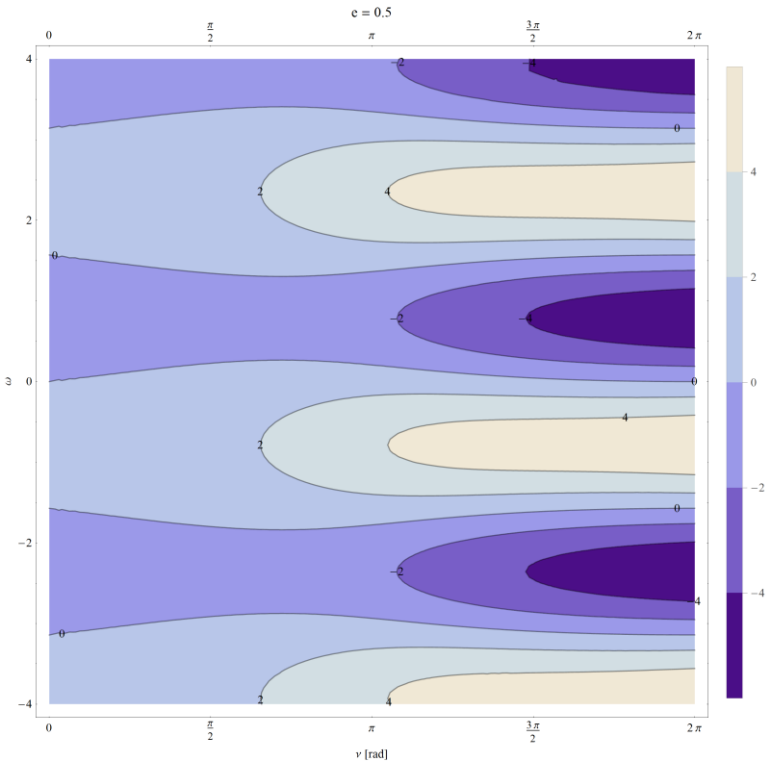

Figure 4.2.1.11 Tether logarithmic ratio - Contour Plot for $e = 0.5$

Analyzing periodicity in this case is not in question, as the error of the approximation is quite large, as seen in Figure 4.2.1.8.

Chapter 5 – Stability conditions

In the following chapter, the monodromy matrix is obtained to analyze stability with respect to small perturbations ($\delta\varphi$) of the orientation angle φ.

Consider the equation studied in Section 4.1:

$$\varphi = \omega\, \nu + \varphi_0 \tag{44}$$

Analyzing the neighborhood of the point $\varphi_0 = 0$, it follows:

$$\varphi = \omega\, \nu + \delta\varphi \tag{45}$$

Substituting Equations (40) and (45) to Equation (36), one obtains

$$(1 + e\cos\nu)\delta\varphi'' + 3\sin(\omega\nu + \delta\varphi)\cos(\omega\nu + \delta\varphi) - \frac{3(1+\omega+\delta\varphi')}{1+\omega}cos(\omega\nu)sin(\omega\nu) = 0 \tag{46}$$

or the nonlinear equation of perturbed motion [34]. The linearized equation is obtained through trigonometric simplifications, with the above equation being rewritten as:

$$(1 + e\cos\nu)\delta\varphi'' + \frac{3}{2}\left(2\cos(2\omega\nu)\delta\varphi - \frac{\sin(2\omega\nu)\delta\varphi'}{1+\omega}\right) = 0 \tag{47}$$

Equation (47) is the equation in variations. It is now possible to analyze its stability using the Floquet theory [40], as this equation is a linearized differential equation of the second order with periodic coefficients. The linearized equation constricts this analysis to small variations of φ. Applying Floquet theory, it is necessary to find the monodromy matrix for this equation.

5.1 Monodromy Matrix

Consider now a system of equations $\boldsymbol{y} = A\boldsymbol{x}$. For the following purpose, observe the change of variables:

$$\delta\varphi = X_1$$
$$\delta\varphi' = X_2$$

The system can be written as:

$$\begin{bmatrix} X_1{}' \\ X_2{}' \end{bmatrix} = A \begin{bmatrix} X_1 \\ X_2 \end{bmatrix} \quad (48)$$

$$\begin{bmatrix} X_1{}' \\ X_2{}' \end{bmatrix} = \begin{bmatrix} 0 & 1 \\ -\dfrac{3cos(2\,\omega\,\nu)}{1+e\,cos\,\nu} & \dfrac{3\,sin(2\,\omega\,\nu)}{2(1+\omega)(1+e\,cos\,\nu)} \end{bmatrix} \begin{bmatrix} X_1 \\ X_2 \end{bmatrix} \quad (49)$$

Some steps have to be done to obtain the monodromy matrix, based on Floquet theory [40]:

1. Do a loop, where variations occur for:
    a. ω, from -4 to 4, and
    b. e, from 0 to 1

and include the next steps.

2. Resolve the numerical ordinary differential equations, substituting firstly:
    a. $X_1 = 0 \;\; and \;\; X_2 = 1$

and secondly,

    b. $X_1 = 1 \;\; and \;\; X_2 = 0.$

Call the solutions given by a. as $\begin{bmatrix} a1 \\ a2 \end{bmatrix}$ and the solutions given by b. as $\begin{bmatrix} b1 \\ b2 \end{bmatrix}$.

3. Create a matrix $B[\nu, \omega, e]$ where the solution of 2.a. and 2.b. are as follow:
    a. $B = \begin{bmatrix} a1 & a2 \\ b1 & b2 \end{bmatrix}$

4. Create the monodromy matrix M, that obeys:
    a. $M[\nu, \omega, e] = 2 - |Tr\ B|$

Note that the creation of B depends on the parameters $\nu, \omega,$ and e. The size of the matrices B and M depends directly with the step size defined for each parameter. Here, the step size of ω and e was chosen $= 0.01$. Since the stability is related with periodicity, the matrix M was plotted below for the value $\nu = 2\pi$. The indicator of stability is given by the ordinate and stability corresponds to Tr B between 0 and 2 $(0 < 2 - |Tr\ B| \leq 2)$, where *Tr* B means Trace of the matrix B. Positive values between the described boundaries correspond to the stability of the solution (linear approximation), negative values correspond to instability and zero values correspond to critical cases. Figures 5.1.1, 5.1.2, 5.1.3 and 5.1.4 represent matrix M, analyzing different ω.

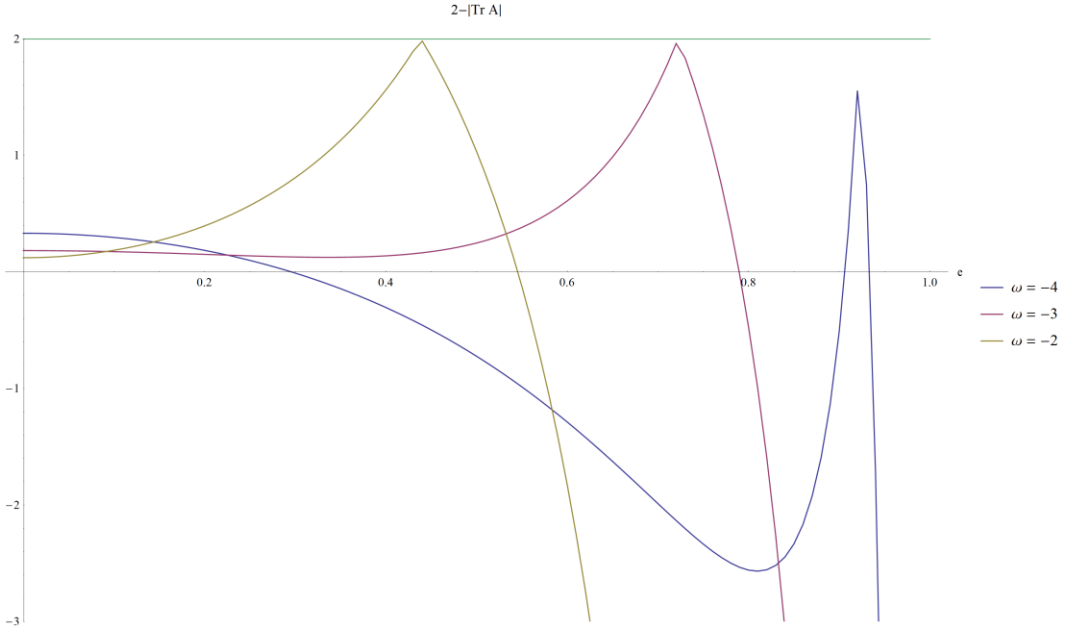

Figure 5.1.1 Stability Indicator for $\omega = \{-4; -3; -2\}$

As it can be seen, in the case where $\omega = \{-4; -3; -2\}$, stability is found for several values of eccentricity, with $\omega = -3$ being the value where stability corresponds to larger intervals of eccentricities.

Fractional numbers can be seen in Figure 5.1.2.

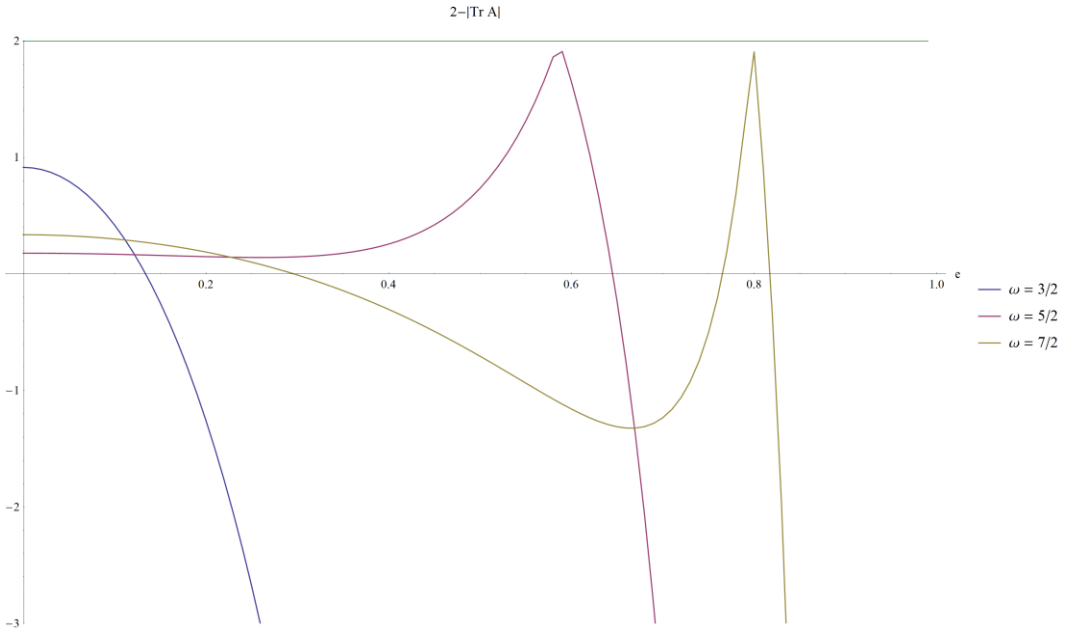

Figure 5.1.2 Stability Indicator for $\omega = \{3/2; 5/2; 7/2\}$

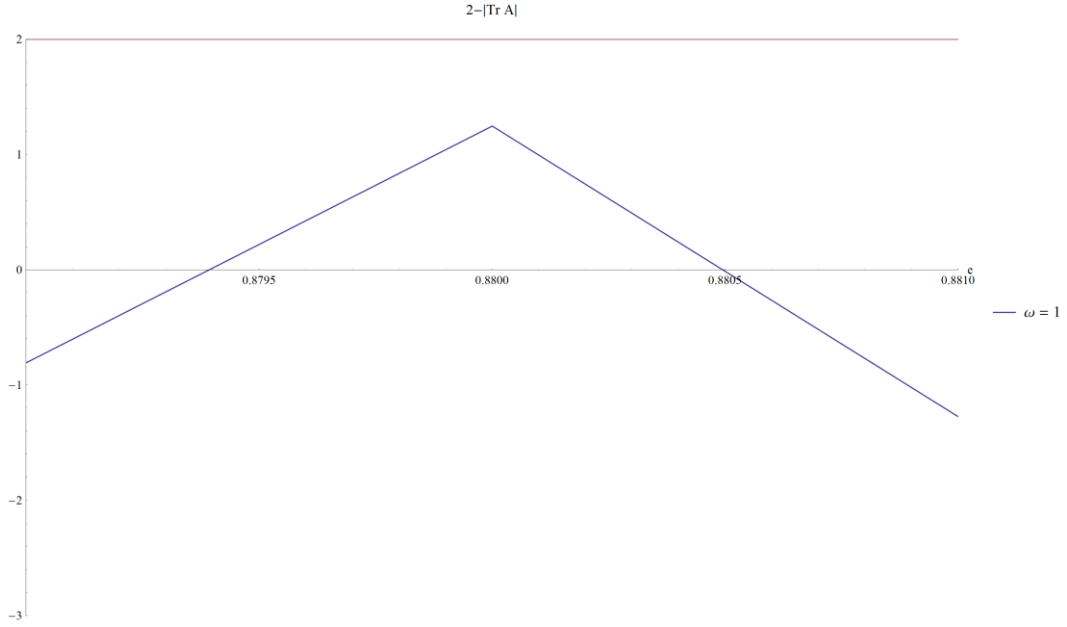

Figure 5.1.3 Stability Indicator for $\omega = 1$

In the case were $\omega = 1$ (Figure 5.1.3), stability is only found for small values of eccentricity.

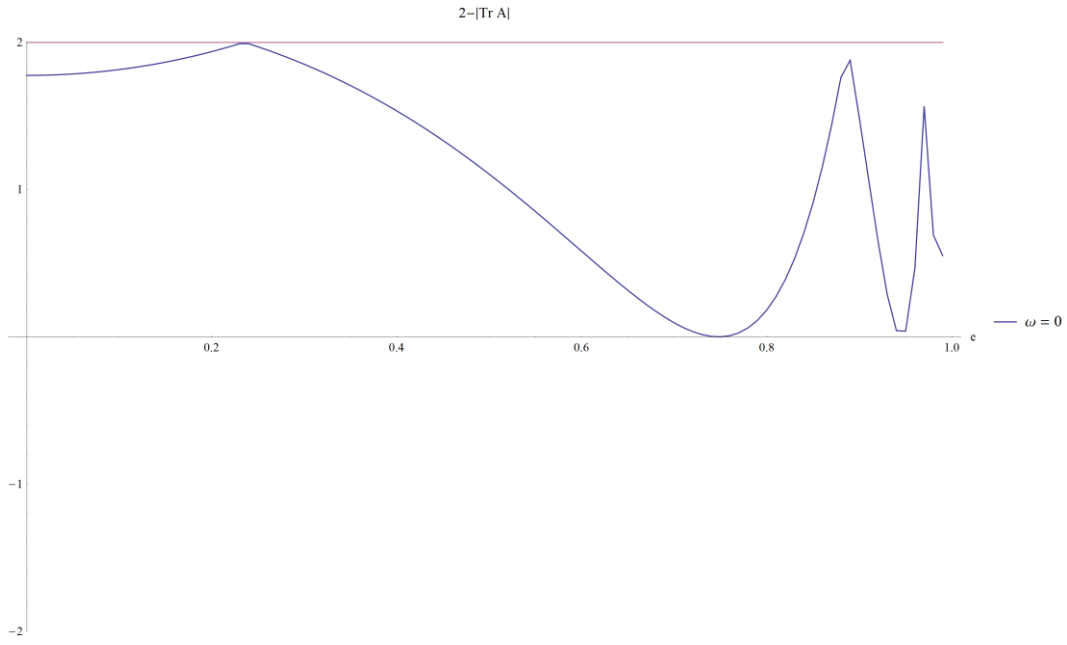

Figure 5.1.4 Stability Indicator for $\omega = 0$

At Figure 5.1.4 ($\omega = 0$), there is a constant stability, having, nonetheless, some critical points around $e \cong 0.25$ and $e \cong 0.75$.

Table 1 shows stability conditions, in function of some values of ω. There are intervals of e values where stability is always met.

Table 1. Stability conditions

Stability Conditions	
$\boldsymbol{\omega}$	Interval of stability for e
0	$e \in [0, 0.99]$
1	$e = 0.88$
2	$e \in]0, 0.55]$
3	$e \in]0, 0.09] U [0.97, 0.98]$
4	$e \in]0, 0.42]$
-2	$e \in]0, 0.54]$
-3	$e \in]0, 0.78]$
-4	$e \in]0\ , 0.29] U [0.91, 0.93]$
Precison: 2 decimal cases	

Those values have been obtained independently of the other system's parameters, like mass of the bodies, or gravitational force.

A contour plot of the stability range in function of ω and e can be seen in Figure 5.1.5. The figure shows the values where stability is found and complements Table 1.

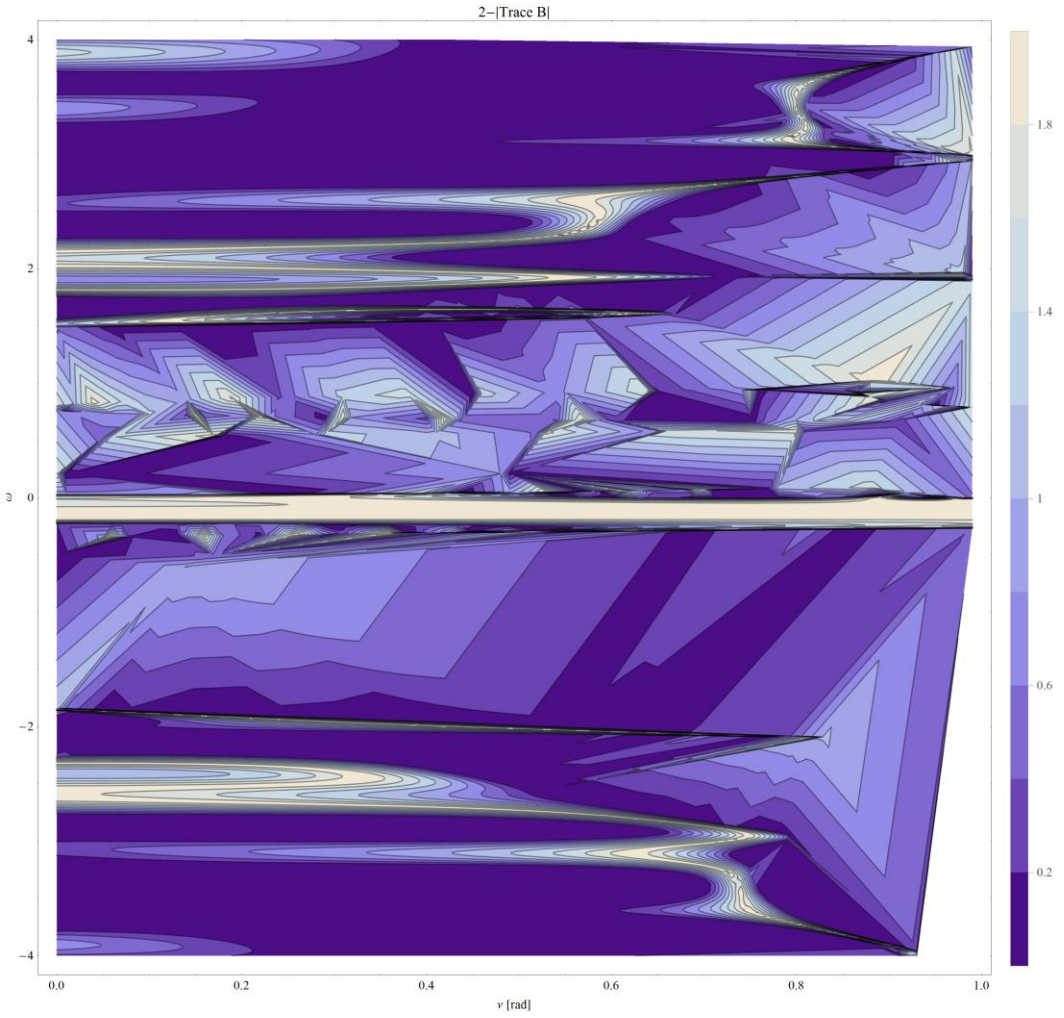

Figure 5.1.5 Contour Plot of the different values of stability

Chapter 6 - Simulations

Simulations are quite important for mission conceptualization. They allow one to verify all the consequences of previous work. A 2D simulator has been created to verify the properties of the system motion. To be able to explore the dynamic demonstration with control features, a free plugin from *Wolfram Mathematica*, called CDF Player (http://www.wolfram.com/cdf-player/) should be installed.

6.1 Dynamic Behavior

Some images have been taken of the simulator, and are shown below for different cases/considerations. Short descriptions of each case are presented.

6.1.1 System Earth – Satellite – Ballast

Table 2. System Earth – Satellite – Ballast Properties

System Properties considered	
Satellite's mass	1000 kg
Semi-latus rectum	Geostationary: 29 422 km Navigation: 13 822 km Observation: 6728 km
Eccentricity	0.003
Ballast's mass suggestion	10% satellite's mass

In Figure 6.1.1.1 a simulation of a geostationary satellite and a counterweight (ballast) can be seen, and a zoom on the moving points can be seen at Figure 5.1.1.2. The satellite mass is chosen to be 1000 kg, and the ballast possesses variable mass (with a limit). The control for choosing a geostationary, a navigation, or an observation satellite can only be seen in the system Earth – Satellite – Ballast.

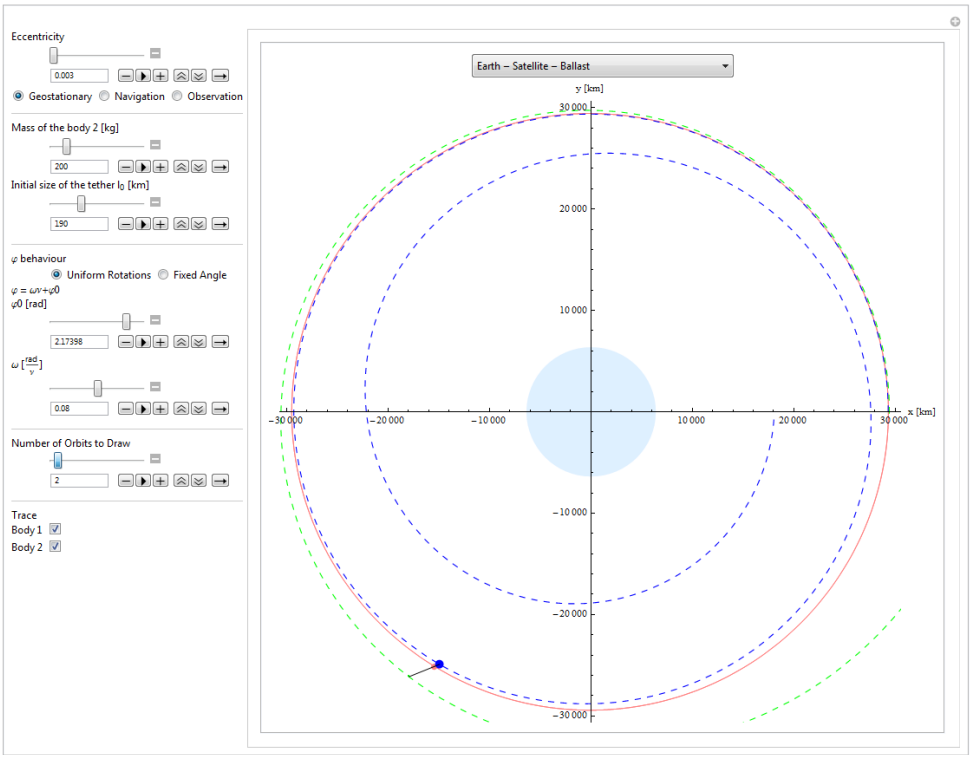

Figure 6.1.1.1 Geostationary Satellite Simulation with $m_2 = 200\ kg, l_0 = 190\ km, \varphi = 0.08v + 2.17398, Orbit\ number = 2$

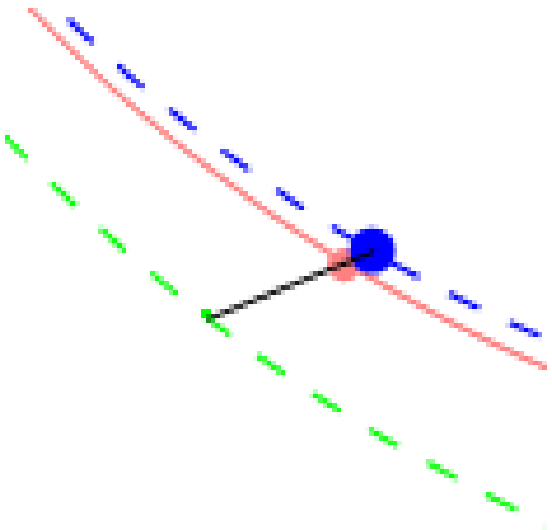

Figure 6.1.1.2 Geostationary Satellite Simulation zoom with $m_2 = 200\ kg, l_0 = 190\ km, \varphi = 0.08v + 2.17398, Orbit\ number = 4$

Figure 6.1.1.1 and Figure 6.1.1.2 show, in dark blue color, the mass point of the satellite, in green the counterweight and in pink the position of the center of mass. Each point has a dashed line that follows its motion in the same color of the respective point.

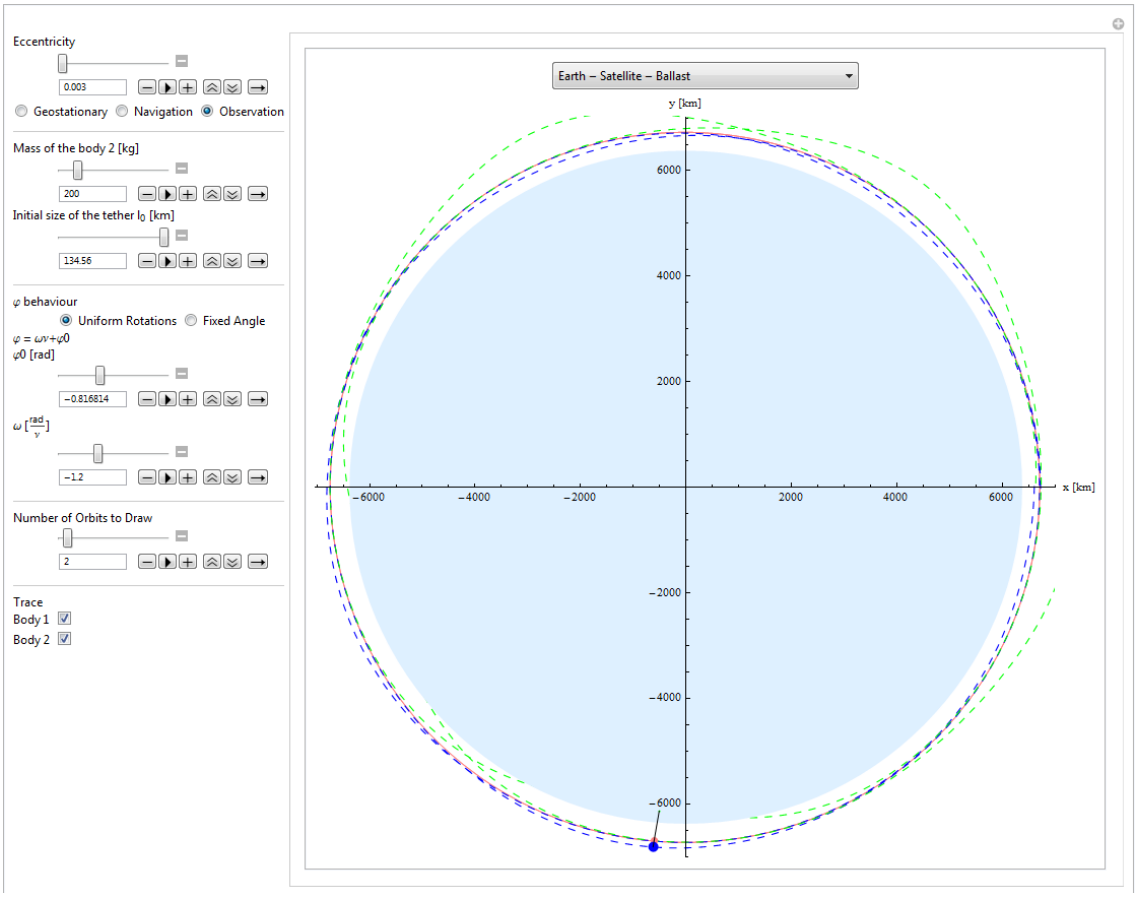

Figure 6.1.1.3 Observation Satellite Simulation with $m_2 = 200\ kg, l_0 = 134.56\ km, \varphi = -1.2v - 0.816814, Orbit\ number = 2$

Figure 6.1.1.3 shows simulation for the same system from an observation orbit. It can be seen that the tether is too long, as it crosses the Earth.

6.1.2 System Earth – Moon - Ballast

This system is a simplification of the Space Elevator. For a Moon Space Elevator, it should be remembered that the fixed angle has to be $\varphi = 0$, to allow the system to always be directed through the Earth's center.

Table 3. System Earth – Moon – Ballast Properties

System Properties considered	
Moon's mass	$7.34767309 \times 10^{22}$ kg
Semi-latus rectum	382843 km
Eccentricity	0.0549
Ballast's mass suggestion	10 000 kg

The result can be seen in Figure 5.1.1.4, and shows to be an excellent solution to the Space Elevator. A size limit for the tether is done automatically (limiting the maximum value of the initial size l_0 to 20% of the semi-latus rectum), to obtain the best solution.

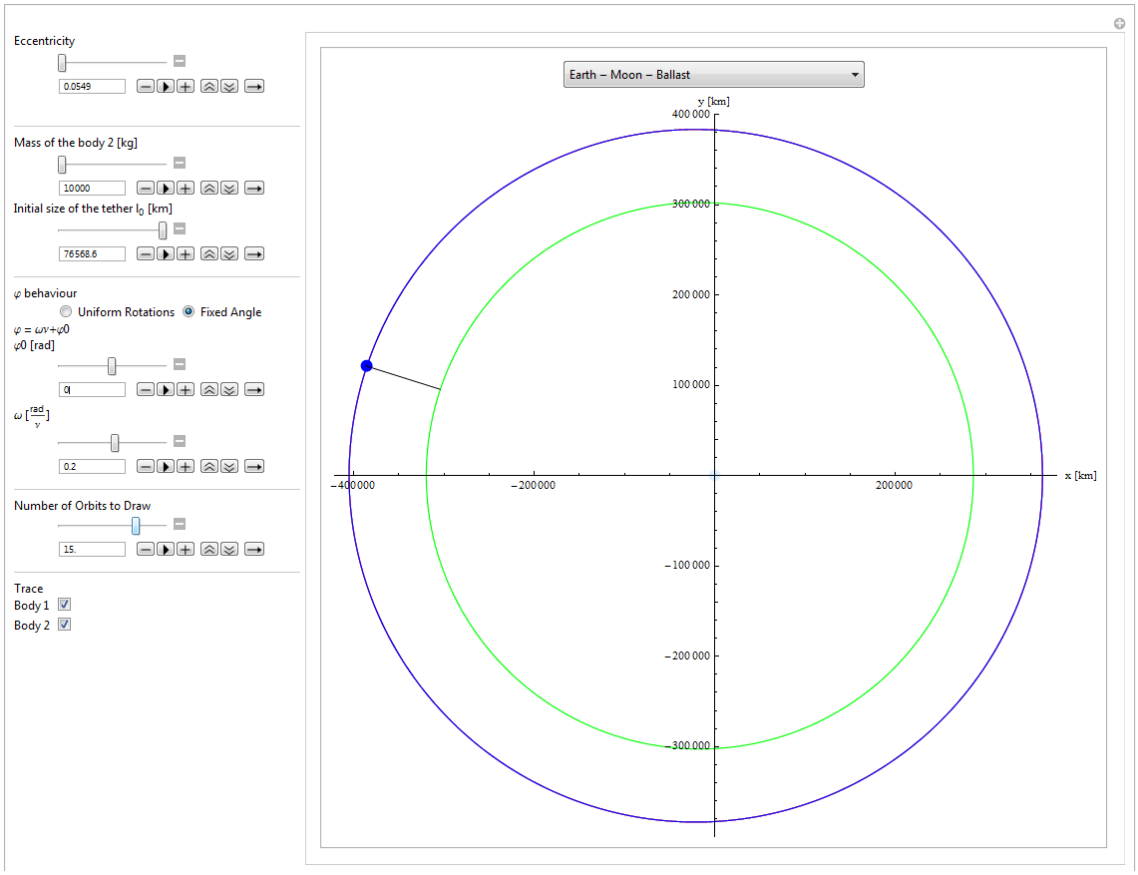

Figure 6.1.2 Earth - Moon - Ballast Simulation (Space Elevator) with $m_2 = 10\,000\ kg, l_0 = 20\%\ \text{semi} - \text{latus} - \text{rectum}, \varphi = 0, Orbit\ number = 15$

6.1.3 System Earth – ISS - Space Module

In this case, the International Space Station (ISS) and a (fictitious) Space Module are simulated (Figure 6.1.3.1). The properties of the system are represented in Table 4.

Table 4. System Earth – ISS – Space Module Properties

System Properties considered	
ISS's mass	50 000 kg
Semi-latus rectum	6799 km
Eccentricity	0.0004123
Ballast's mass suggestion	1 000 kg

In this simulation it is possible to see that the center of mass is always moving in the same path, but small position's variations of the ISS (dark blue point) do make considerable changes in the Space Module motion (as the green path suggests).

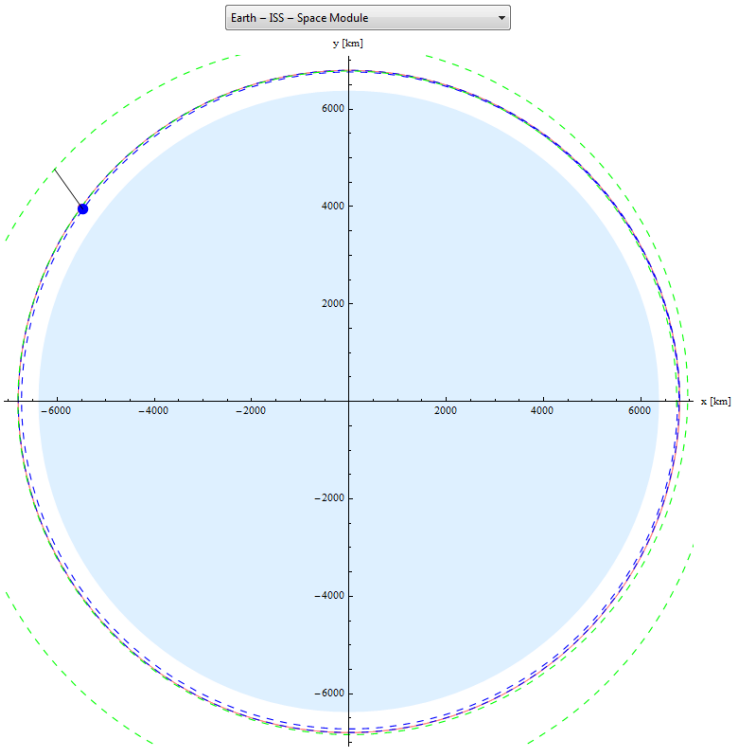

Figure 6.1.3.1 ISS Simulation Zoom with $m_2 = 3000\ kg, l_0 = 130\ km, \varphi = 0.2\ v + 1.05558, Orbit\ number = 2$

Consider now the same system (Figure 6.1.3.2), but with the Space Module weighing 15 000 kg. The non-rotating option is activated now (fixed angle) and the satellite points always to the center of the Earth. After 20 orbits, the bodies describe the same path.

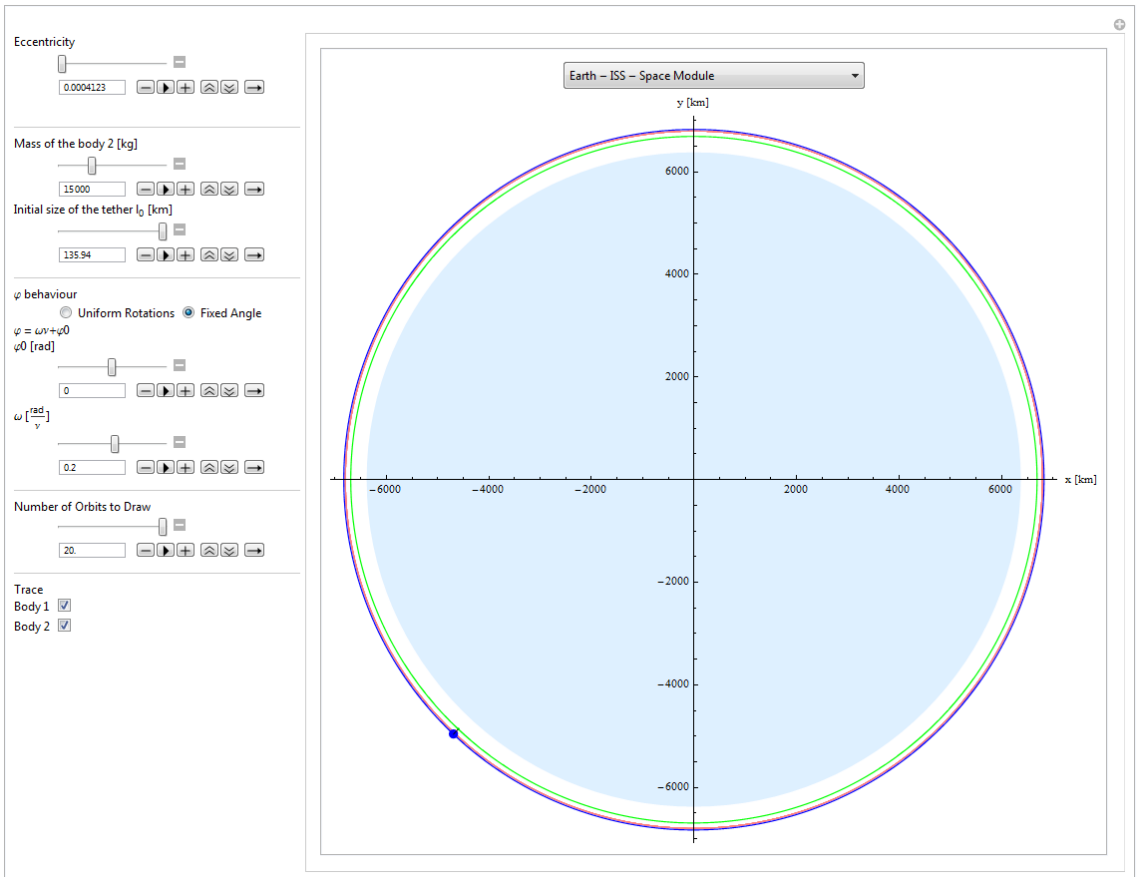

Figure 6.1.3.2 ISS Simulation with $m_2 = 15000\ kg, l_0 = 135.94\ km, \varphi = 0, Orbit\ number = 20$

6.1.4 System Moon – SMART1 – Satellite

SMART 1 [41] is a satellite of ESA (European Space Agency) that orbited Moon. A simulation of this satellite connected with another one can be seen in Figure 6.1.4.

Table 5. Moon – SMART1 – Satellite Properties

System Properties considered	
SMART1's mass	2130 kg
Semi-latus rectum	1838 km
Eccentricity	0.003
Ballast's mass suggestion	1000 kg

In Figure 6.1.4, the trace of the second satellite is omitted. The simulation shows that the parameters (like mass and tether length) of the mission SMART1 are executable.

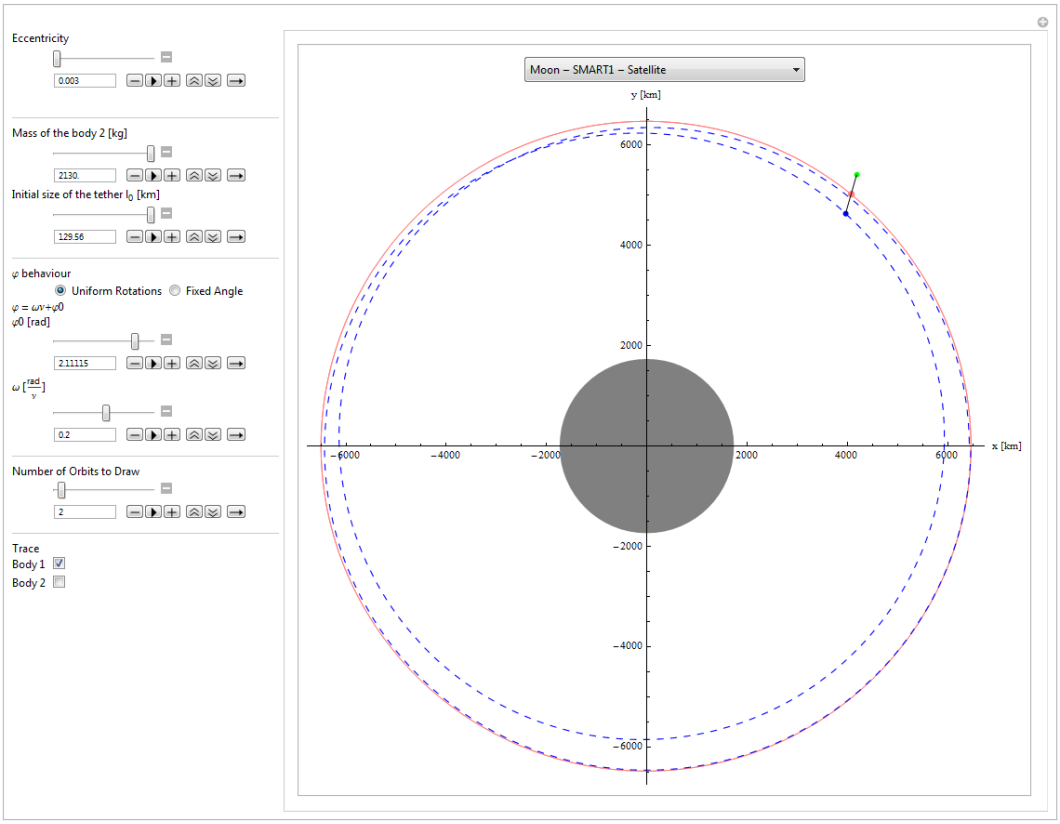

Figure 6.1.4 SMART1 Simulation with $m_2 = 2130\ kg, l_0 = 129.56\ km, \varphi = 0.2v + 2.11115, Orbit\ number = 2$

6.1.5 System Titan – SST1 – SSTM

Two fictitious modules have been studied, namely SST1 (Space System in Titan 1) and SSTM (Space System in Titan – Module), as seen in Figures 6.1.5.1 and 6.1.5.2.

Table 6. System Titan – SST1 – SSTM Properties

System Properties considered	
SST1's mass	2130 kg
Semi-latus rectum	3575 km
Eccentricity	0.0288
Ballast's mass suggestion	100 kg

Although it is almost imperceptible, the variations of ω create a wave effect variation in the system positions for this case. It can only be seen in the animation.

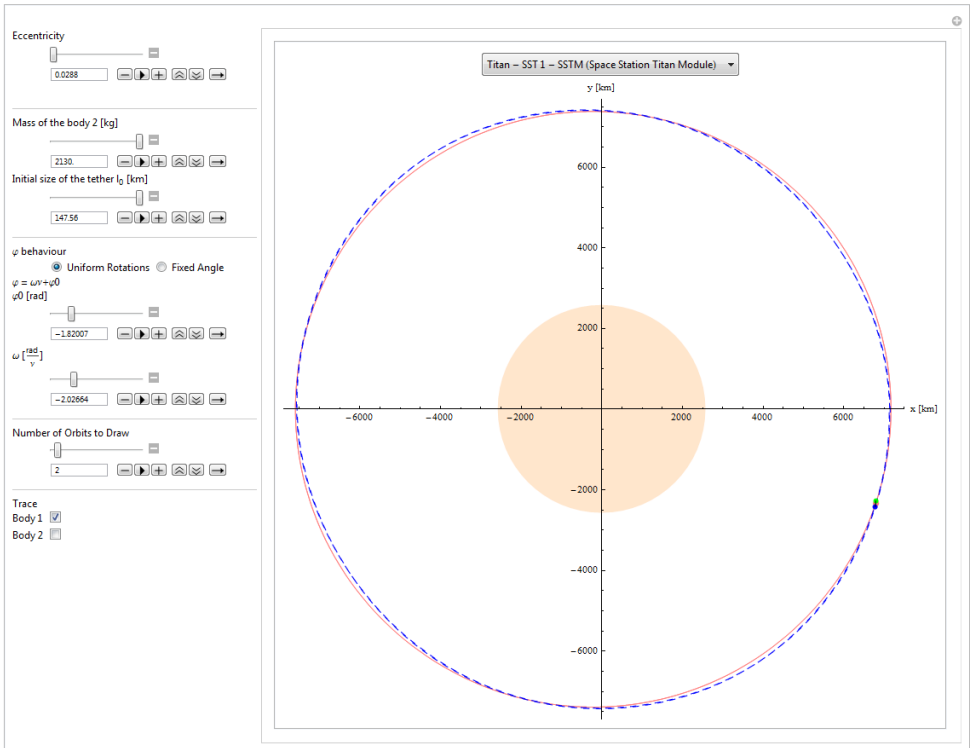

Figure 6.1.5.1 SST1 Simulation with $m_2 = 100\ kg, l_0 = 147.56\ km, \varphi = -2.02664v - 1.82007, Orbit\ number = 2$

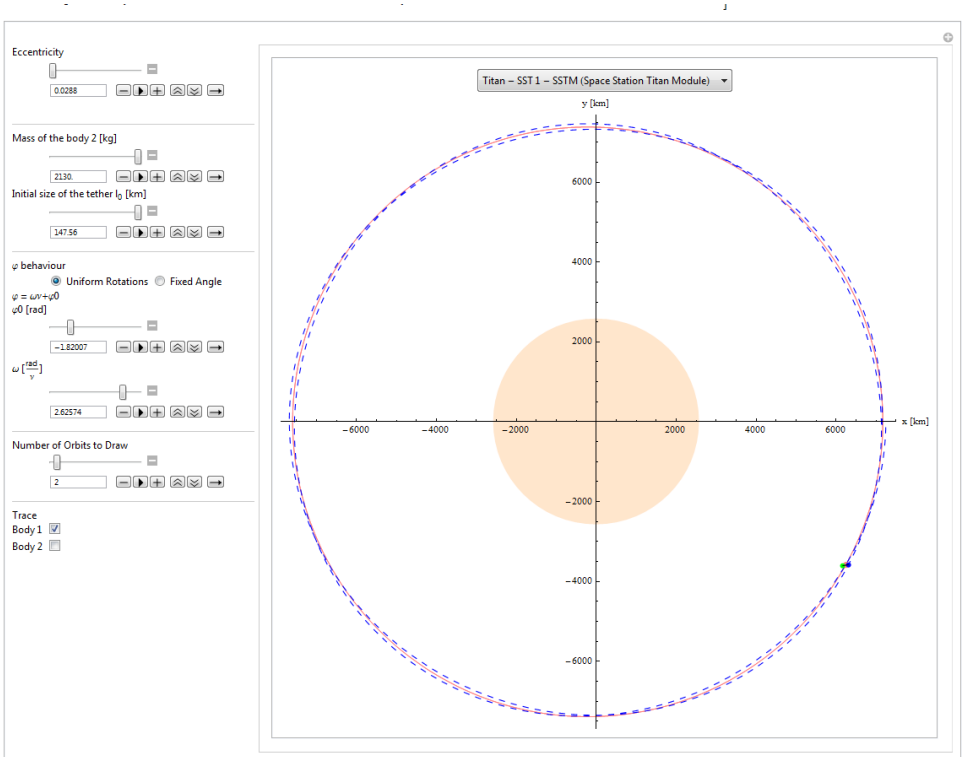

Figure 6.1.5.2 SST1 Simulation with $m_2 = 100\ kg, l_0 = 147.56\ km, \varphi = 2.62574 - 1.82007, Orbit\ number = 2$

In all the presented simulations, the values of some parameters are chosen beforehand, but can be changed any time. These options are helpful to analyze the system and can even serve to understand the meaning of the stability conditions, as Chapter 5 predicts.

6.2 Tether actuating force

As it has been noted before, the only force actuating on the system is the gravitational attraction. As Hao Wen *et al.* refer in [16], the force in the tether can be calculated as:

$$T_{Force} = \frac{\mu * m_1 * m_2}{{r_1}^2 * {r_2}^2} * \frac{{r_2}^3 - {r_1}^3}{m_1 * r_1 + m_2 * r_2} \qquad (50)$$

For a numerical analysis of the influence of the gravitational force on the tether, it can be seen as a function of ν (Figures 6.2.1, 6.2.2, and 6.2.3).

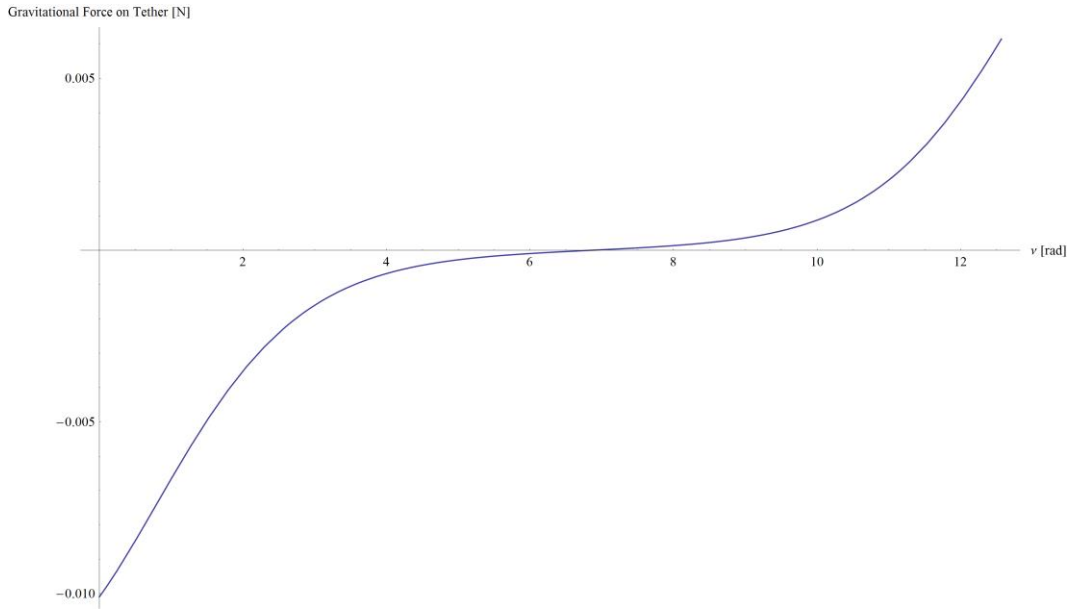

Figure 6.2.1 Earth – Satellite – Ballast variation force in function of ν for $m_2 = 200\ kg, l_0 = 130\ km, \varphi = 0.2\nu + 0.2, Orbit\ number = 4$

As Figure 6.2.1 shows, the force is small, which corresponds to the expectations, as the two-body masses are small. For the ISS system, for example, considering a space module of 10 000 kg, the force actuating in the tether is seen in Figure 6.2.2:

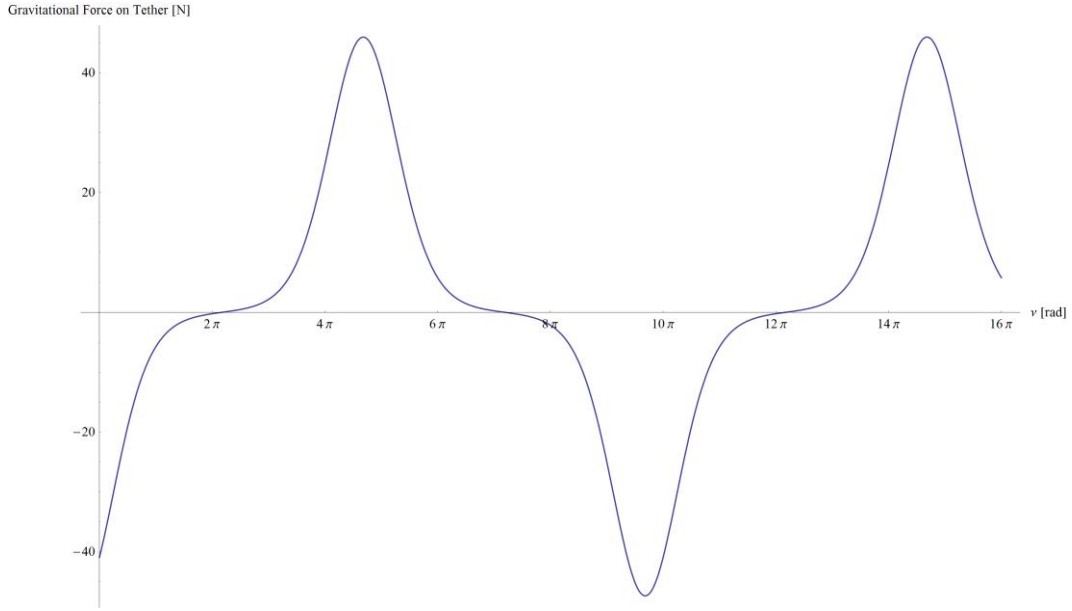

Figure 6.2.2 Earth – ISS – Space Module with $m_2 = 10\ 000\ kg, l_0 = 130\ km, \varphi = 0.2\nu + 0.2, Orbit\ number = 4$

The maximum value of the tether force appears at $\nu = 9.54\,\pi$, and reaching 46.15 N (compression). In every simulation, increasing the initial size of the tether and/or the mass of the second body will increase the order of values of the force actuating on the tether. The parameters chosen for φ also change the force values, as can be seen in Figure 6.2.3:

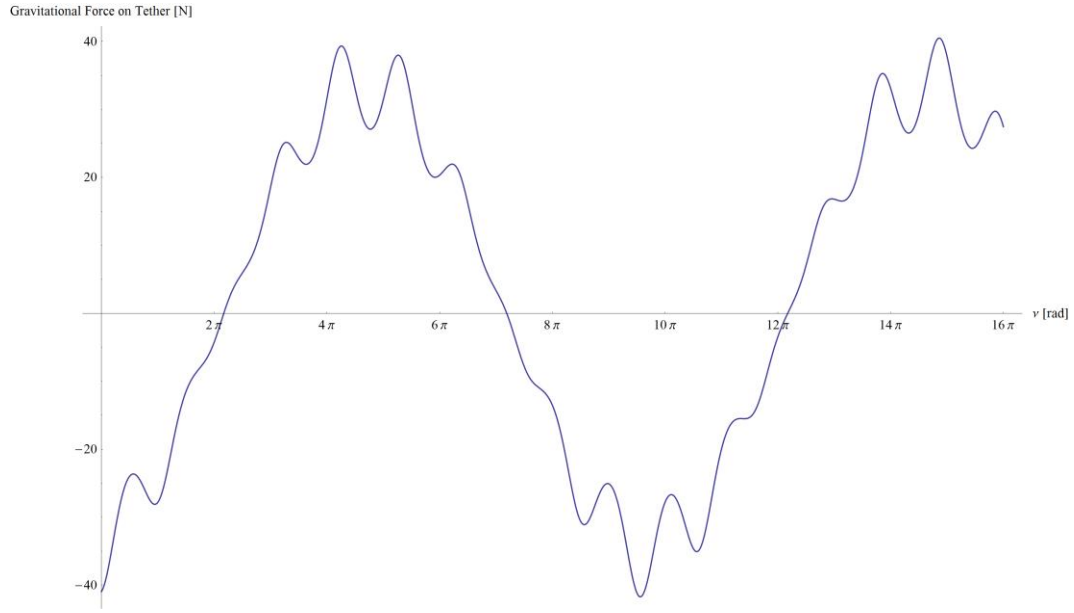

Figure 6.2.3 Earth – ISS – Space Module with $m_2 = 10\,000\,kg, l_0 = 130\,km, \varphi = 0.94\nu + 0.0628319, Orbit\ number = 4$

This means that the control law of φ has a direct impact on the forces applied to the tether.

6.3 Energy analysis

Analysis of the energy balance allows one to perform the global analysis of the system. The kinetic and potential energies can be seen in Figure 6.3.1 and Figure 6.3.2.

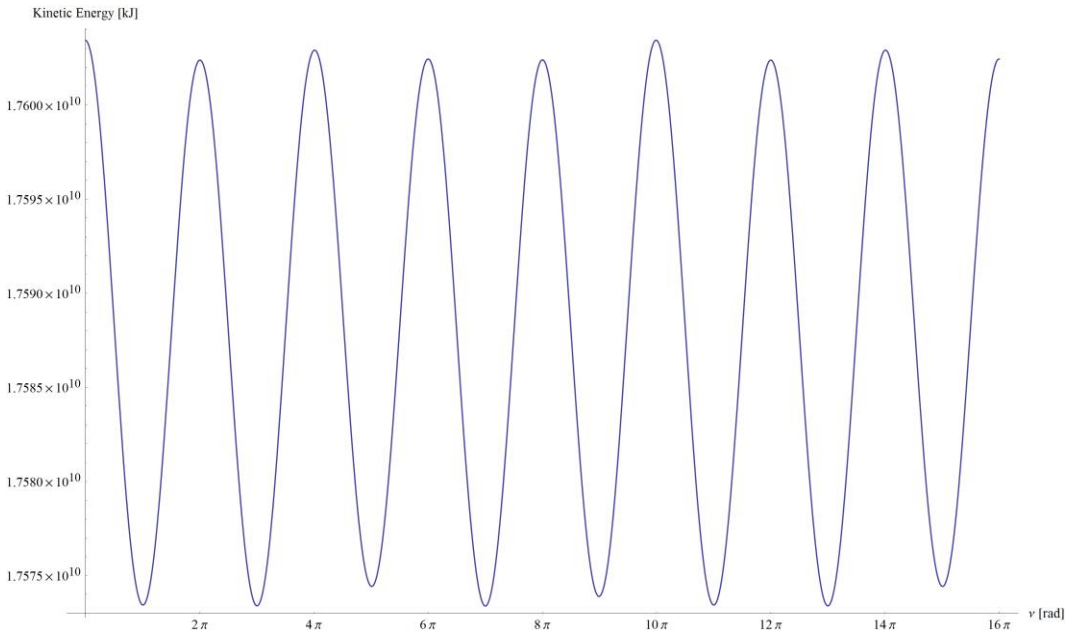

Figure 6.3.1 Kinetic energy for System Earth – ISS – Space Module with $m_2 = 10\,000\ kg, l_0 = 130\ km, \varphi = 0.2\nu + 0.2, Orbit\ number = 8$

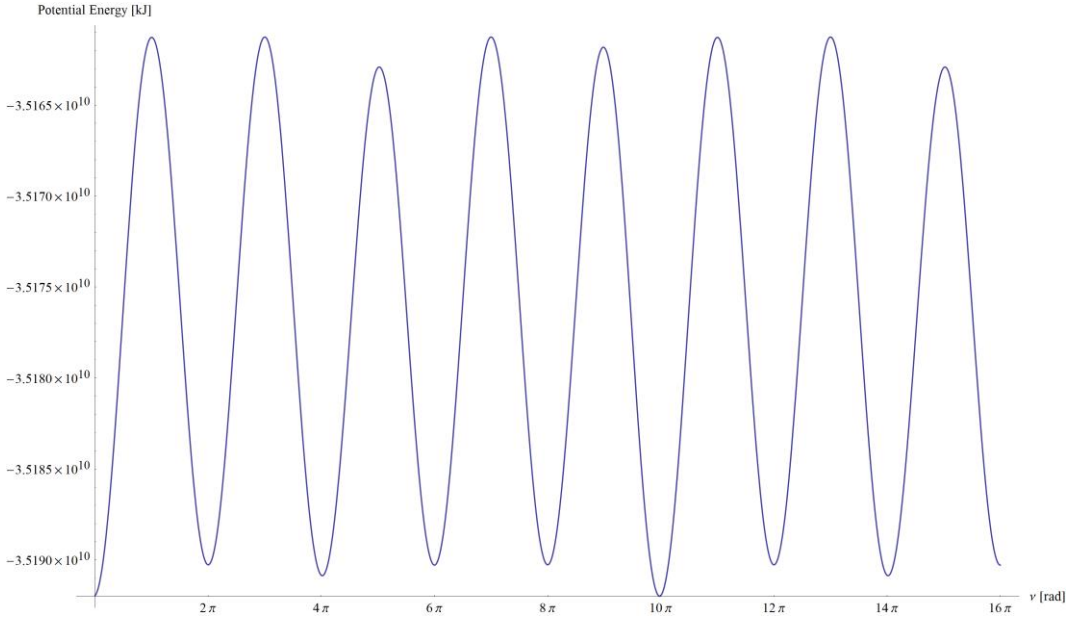

Figure 6.3.2 Potential energy for System Earth – ISS – Space Module with $m_2 = 10\,000\ kg, l_0 = 130\ km, \varphi = 0.2\nu + 0.2, Orbit\ number = 8$

Kinetic and potential energies tend to oscillate, and inverse to each one, which has been expected, as it is a conservative system.

Chapter 7 – Conclusions

We consider here dynamics of a two-body tethered satellite system in an elliptic geocentric orbit. The satellites are represented as massive points connected by a light rigid link. The tether length is assumed to be small compared to the orbit dimensions, so the orbit of the system center of mass is supposed to be Keplerian. To describe the system motion, we deduce the respective Lagrangian equations. These equations are used to find the control law for the tether length that causes some programmed attitude motion of the tethered system.

We consider two types of the programmed motion: the uniform rotations of the tether and the permanent orientation of the tether with respect to the local vertical. Substitution of the law of motion to the Lagrangian equation permits us to obtain the differential equation for the control; its analytical integration is not always possible and the following study is done combining numerical analysis and approximation.

The numerical simulations of the system dynamics show that it is possible to use changes of the tether's length to keep uniform rotation of the tether, as well as its permanent orientation with respect to the local vertical. The only exception is the case of $\omega = -1$ that corresponds to a fixed orientation of the tether in the absolute space. For all other values of the tether's angular velocities, including the case $\omega = 0$ (a fixed orientation with respect to the local vertical), one can find the control law $l = l(\nu)$ that implements the referred motion. Such control laws can be 2-π periodic for integral values of ω; for some values the control laws are not periodic.

For small values of eccentricity *e* the control law can be found analytically using the Taylor series. The resulting closed-form solutions are rather cumbersome, but quite accurate for small *e* as they practically coincide with the numerically obtained control laws.

Stability of the permanent rotations has been studied using the Floquet theory. The intervals of eccentricity where the stability conditions hold true have been found for a number of angular velocities.

For the permanent orientations with respect to the local vertical, it is found that the orientation keeping along the whole orbit is possible only for some specific values of the orientation angle φ, e.g., for $\varphi = 0$. For other configurations, the control laws are discontinuous making it impossible to implement the respective motion at least at a part of the orbit.

To provide the visualization of the obtained results and to facilitate the perception of the system dynamics, a numerical simulator of the tethered connected system has been implemented using the Mathematica 9 software. The simulations performed using this tool

confirm the previously obtained results. In addition, several tethered system with realistic parameters have been simulated and their dynamics studied and visualized.

The analysis presented here show a number of important properties of two-body tethered systems. However, it is based on a simplified model that neglects the mass of the tether and its flexibility and elasticity, as well as several perturbations, such as aerodynamics forces and solar pressure. The future work should implement a more realistic system model. The other possible direction of the research is connected with the analysis of large-scale tether system dynamics, when the orbital motion of the system cannot be separated from its attitude dynamics.

Bibliography

[1] V. Kaithi, "Design of Space Elevator," Texas, 2008.

[2] J. Arneson, "Konstantin Tsiolkovsky," March 2007. [Online]. Available: http://www.thelivingmoon.com/45jack_files/03files/Tsiolkovsky_001_Intro.html. [Accessed 14 September 2013].

[3] C. W. Swan and P. A. Swan, "Why we need a space elevator," *Space Policy,* vol. 22, pp. 86-91, April 2006.

[4] G. Dvorsky, "Why we'll probably never build a space elevator," February 2013. [Online]. Available: http://io9.com/5984371/why-well-probably-never-build-a-space-elevator. [Accessed 13 September 2013].

[5] B. C. Edwards and E. A. Westling, The Space Elevator: A Revolutionary Earth-to-Space Transportation System, BC Edwards, 2003.

[6] V. V. Beletsky and E. M. Levin, Dynamics of space tether systems, vol. 83, American Astronautical Society, 1993.

[7] M. P. Cartmell and D. J. McKenzie, "A review of space tether research," *Progress in Aerospace Sciences,* vol. 44, pp. 1-21, November 2008.

[8] M. L. Cosmo and E. C. Lorenzini, Tethers in Space Handbook, Cambridge, Massachusetts: Smithsonian Astrophysical Observatory, 1997.

[9] M. v. Pelt, Space tethers and space elevators, Springer, Ed., Copernicus Books, 2009.

[10] J. H. Hoffman, A. Mazzoleni and A. Santangelo, *Design of an Artificial Gravity Generating Tethered Satellite System,* New Mexico: American Institute of Physics, 2001.

[11] N/A, "Nasa Science Missions," NASA, [Online]. Available: http://science.nasa.gov/missions/tss/. [Accessed 23 February 2014].

[12] K. Fluegel, "Johnson Space Center," NASA, 25 June 1993. [Online]. Available: http://www.nasa.gov/centers/johnson/news/releases/1993_1995/93-049.html. [Accessed 23 February 2014].

[13] Y. Chen, R. Huang, X. Ren, L. He and Y. He, "History of the Tether Concept and Tether Missions: A Review," *ISRN Astronomy and Astrophysics,* vol. 2013, 16 January 2013.

[14] G. Zhai and Z. Jing-rui, "Space Tether Net System for Debris Capture and Remov l," in *4th International Conference on Intelligent Human-Machine Systems and Cybernetics*, Nanchang, China, 2012.

[15] O. L. d. Weck, "Attitude Determination and Control (ADCS)," 2001. [Online]. Available: http://ocw.mit.edu/courses/aeronautics-and-astronautics/16-851-satellite-engineering-fall-2003/lecture-notes/l9_acs.pdf. [Accessed 11 February 2013].

[16] H. Wen, D. P. Jin and H. Y. Hu, "Advances in dynamics and control of tethered satellite systems," *Acta Mech Sin,* vol. 24, pp. 229-241, 2008.

[17] J. Ashenberg and E. C. Lorenzini, "Active gravity-gradient stabilization of a satellite in elliptic orits," *Acta Astronautica,* vol. 45, no. 10, pp. 619-627, March 1999.

[18] M. Pascal, A. Djebli and L. E. Bakkali, "Laws of deployment/retrieval in tether connected satellites systems," *Acta Astronautica,* vol. 45, no. 2, pp. 61-73, 1999.

[19] M. Pascal, "On fast retrieval laws for tethered satellite systems," *Acta Astronautica,* vol. 50, no. 8, p. 461–470, 2002.

[20] B. C. Edwards, "The Space Elevator," NASA Institute for Advanced Concepts, 2000.

[21] A. Djebl and M. Pascal, "A new method for the orbital modification of a tether connected satellite system," *Acta Mechanica,* vol. 167, pp. 113-122, 2004.

[22] J. Pekka, J.-P. Lebreton, S. Merikallio, M. Paton, G. Mengali and A. A. Quarta.

[23] A. Pukniel, V. Coverstone, R. Burton and D. Carroll, "The dynamics and control of the CubeSail mission: A solar sailing demonstration," *Advances in Space Research,* vol. 48, pp. 1902-1910, 2011.

[24] A. K. Misra, Z. Amier and V. J. Modi, "Attitude dynamics of three-body tethered systems," *Acta Astronautica,* vol. 17, no. 10, pp. 1059-1068, 1988.

[25] K. Kumar and K. D. Kumar, "Tethered dual spacecraft configuration: a solution to attitude control problems," *Aerospace Science and Technology,* vol. 4, pp. 495-505, 2000.

[26] A. D. Guerman, "Equilibria of multibody chain in orbit plane," *Jorunal of Guidance, Control and Dynamics,* vol. 26, no. 6, pp. 942-948, 2003.

[27] A. D. Guerman, "Spatial equilibria of multibody chain in a circular orbit," *Acta Astronautica,* vol. 58, no. 1, pp. 1-14, 2006.

[28] A. D. Guerman, "Stationary configurations of tetrahedral tethered satellite formation," *Journal of Guidance, Control and Dynamics,* vol. 31, no. 2, pp. 424-428, 2008.

[29] S. Yu, "Tethered Satellite System Analysis (1) - two-dimensional case and regular dynamics," *Acta Astronautica,* vol. 47, no. 12, pp. 849-858, 2000.

[30] A. K. Misra, "Dynamics and control of tethered satellite systems," *Acta Astronautica,* vol. 63, pp. 1169-1177, 2008.

[31] W. Dittrich and M. Reuter, "Poincaré Surface of Sections, Mappings," in *Classical and Quantum Dynamics*, Springer, 1994, pp. 155-163.

[32] A. A. Burov, I. I. Kosenko and A. D. Guerman, "Dynamics of a moon-anchored tether with variable length," *Advances in the Astronautical Sciences,* vol. 142, pp. 3495-3507, 2012.

[33] W. Zhang and M. H. Yao, "Periodic solutions and stability of a tethered satellite system," *Mecahnics Research Communications - Elsevier,* vol. 44, pp. 24-29, 2012.

[34] A. A. Burov, I. I. Kosenko and A. D. Guerman, "Uniform rotations of a two-body tethered system in an elliptic orbit," in *64th International Astrounautical Congress*, Beijing, China, 2013.

[35] H. D. Curtis, Orbital Mechanics for Engineering Students, Daytona Beach, Florida: Elsevier, 2010.

[36] A. D. Guerman, Dinâmica dos Sistemas Mecânicos - 1. Métodos da mecânica analítica, Covilhã, 2002.

[37] J. A. Shapiro, Classical Mechanics, 2010.

[38] A. A. Burov, "Oscillations of a Vibrating Dumbbell on an Elliptic Orbit," *Doklady Physics,* vol. 56, no. 3, pp. 182-185, 2011.

[39] A. A. Burov, A. D. Guerman and I. I. Kosenko, "Dynamics of tethered system connected to moon surface," in *DyCoSS - 2nd IAA Conference on Dynamics and Control of Space Systems*, Rome, 2014.

[40] J. Yang, "Basic Floquet Theory," 2011. [Online]. Available: http://www.emba.uvm.edu/~jxyang/teaching/Floquet_theory_Ward.pdf. [Accessed 12 June 2014].

[41] D. P. S. d. Santos, A. B. Prado, L. Casalino and G. Colasurdo, "Optimal trajectories using gravity assisted maneuver and solar electric propulsion (SEP) towards near-earth-objects," *Journal of Aerospace Engineering,* vol. 1, no. 2, p. 51, 2008.

[42] M. Navabi, N. Nasiri and M. Dehghan, "Modeling and numerical simulation of linear and nonlinear spacecraft attitude dynamics and gravity gradient moments: A comparative study," *Commun Nonlinear Sci Numer Simulat,* vol. 17, pp. 1065-1084, 2012.

Annex 1

In Section 2.3 were presented some applications and mission of satellite tether systems. Here, a complete list is shown of important missions (with or without succeeded status).

Table 7. TSS missions till 2013

Mission	Year	Sponsor	Orbit	Length	Status
Gemini XI	1967	NASA	LEO	50 m	Launched
Gemini XII	1967	NASA	LEO	30 m	Launched
TPE-1	1980	NASA/ISAS	Suborbital	400 m	Launched
TPE-2	1981	NASA/ISAS	Suborbital	500 m	Launched
TPE-3 (CHARGE-1)	1983	NASA/ISAS	Suborbital	500 m	Launched
CHARGE-2	1985	NASA/ISAS	Suborbital	500 m	Launched
MAIMIK	1986	NASA/NDRE	LEO	400 m	Launched
ECHO-7	1988	USAF	Suborbital	—	Launched
OEDIPUS-A	1989	NRC/NASA/CRC/CSA	Suborbital	958 m	Launched
CHARGE-2B	1992	NASA/ISAS	Suborbital	500 m	Launched
TSS-1 (STS-46)	1992	NASA/ASI	LEO	267 m	Launched
SEDS-1	1993	NASA	LEO	20 m	Launched
PMG	1993	NASA	LEO	500 m	Launched
SEDS-2	1994	NASA	LEO	20 m	Launched
OEDIPUS-C	1995	NASA/NRC/CRC/CSA	Suborbital	1 km	Launched

TSS-1R (STS-75)	1996	NASA/ASI	LEO	19.6 km	Launched
TSS-2 (STS-75)	1996	NASA	LEO	100 m	Cancelled
TiPS	1996	NRO/NRL	LEO	4 km	Launched
YES	1997	ESA/Delta-Utec	LEO	35 m	Launched
ATEx	1999	NRO/NRL	LEO	22 m	Launched
PICOSATs	2000	Aerospace corporation	LEO	30 m	Launched
MEPSI	2002	Aerospace corporation	LEO	15.2 m	Launched
ProSEDS	2003	NASA	LEO	15 m	Cancelled
MAST	2007	NASA/TUI/Stanford	LEO	1 km	Launched
YES2	2007	ESA/Delta-Utec	LEO	31.7 m	Launched
STARS	2009	Kagawa university	LEO	5 m	Launched
T-REX	2010	ISAS/JAXA	LEO	300 m	Launched
TEPCE	2013	NRO/NRL	LEO	1 km	Planning

Annex 2

In Chapter 4 an analysis was done for φ control laws. The graphics of other simulations done can be seen in the present annex. The following graphics were obtained with the previous substitution of ω and consequent integration.

2.1 Uniform rotations

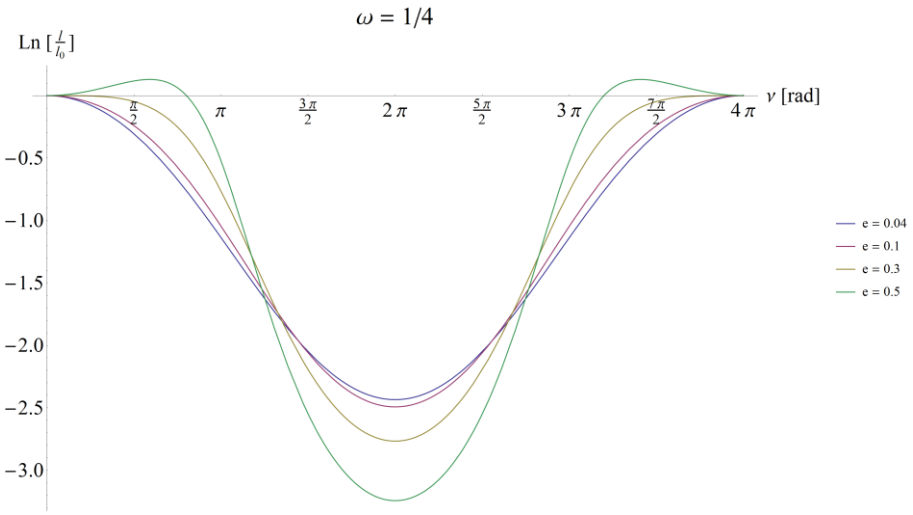

Figure A.2.1 Tether logarithmic ratio for different eccentricities and $\omega = 1/4$

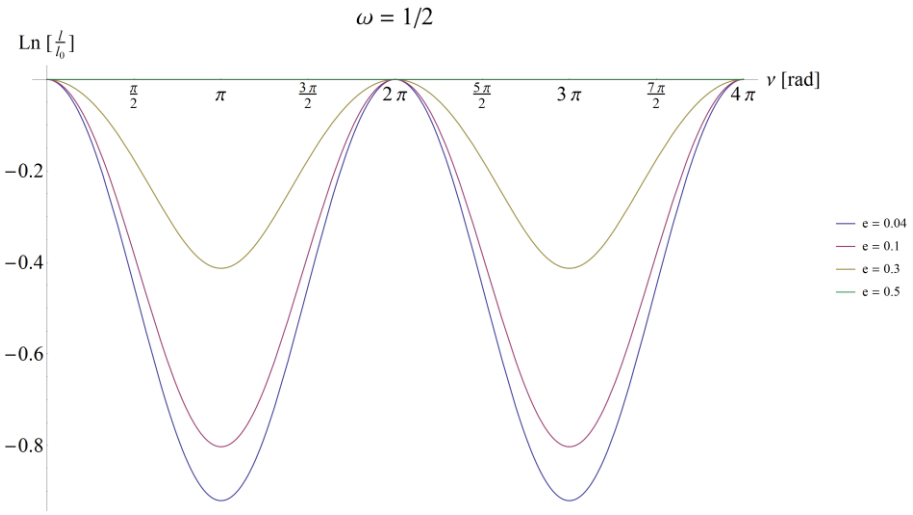

Figure A.2.2 Tether logarithmic ratio for different eccentricities and $\omega = 1/2$

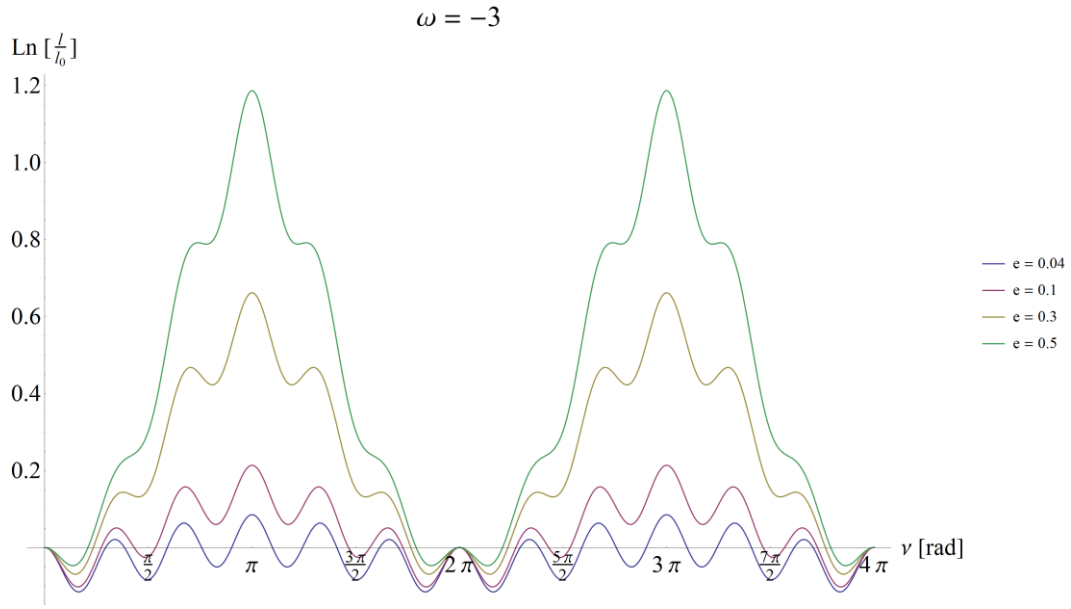

Figure A.2.3 Tether logarithmic ratio for different eccentricities and $\omega = -3$

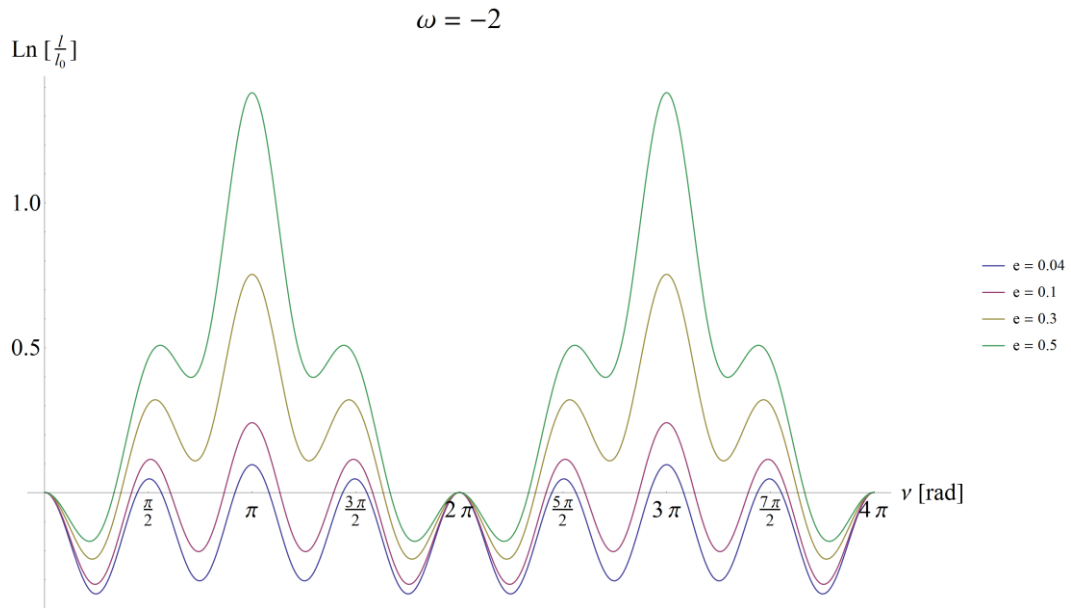

Figure A.2.4 Tether logarithmic ratio for different eccentricities and $\omega = -2$

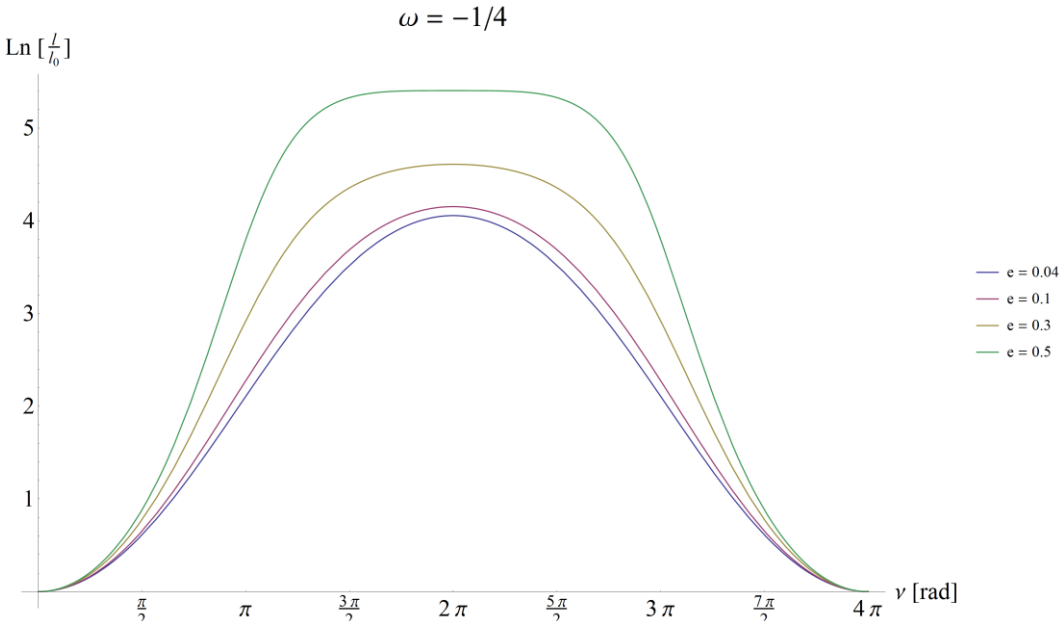

Figure A.2.5 Tether logarithmic ratio for different eccentricities and $\omega = -1/4$

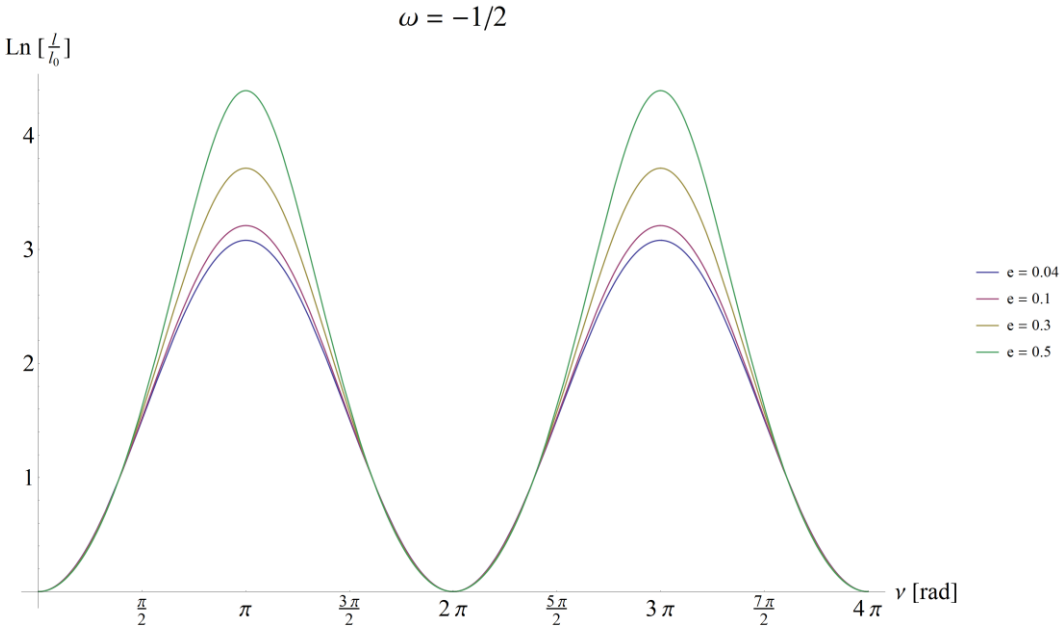

Figure A.2.6 Tether logarithmic ratio for different eccentricities and $\omega = -1/2$

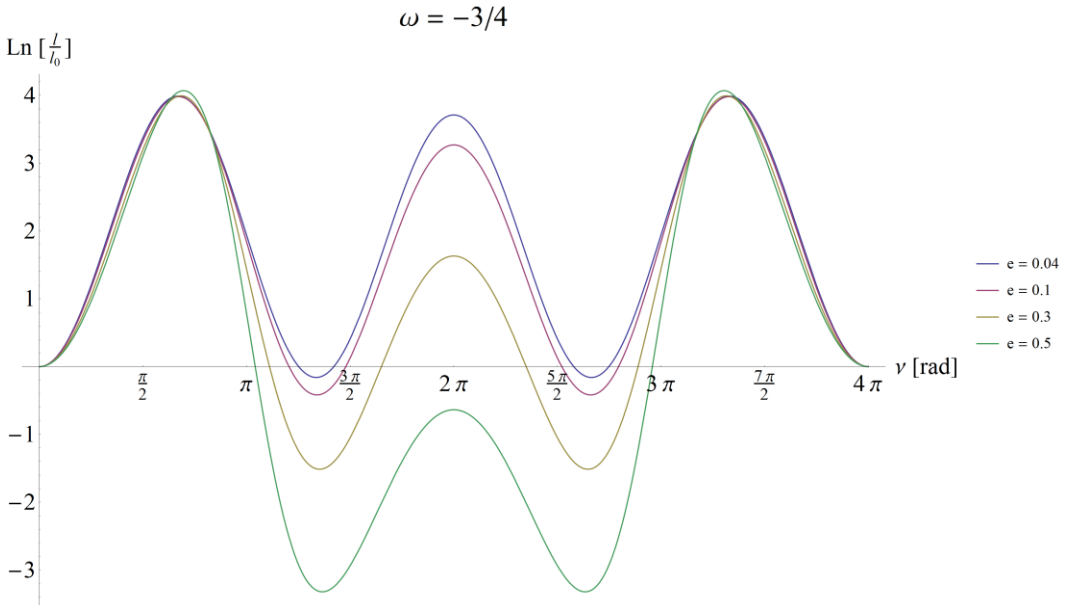

Figure A.2. 7 Tether logarithmic ratio for different eccentricities and $\omega = -3/4$

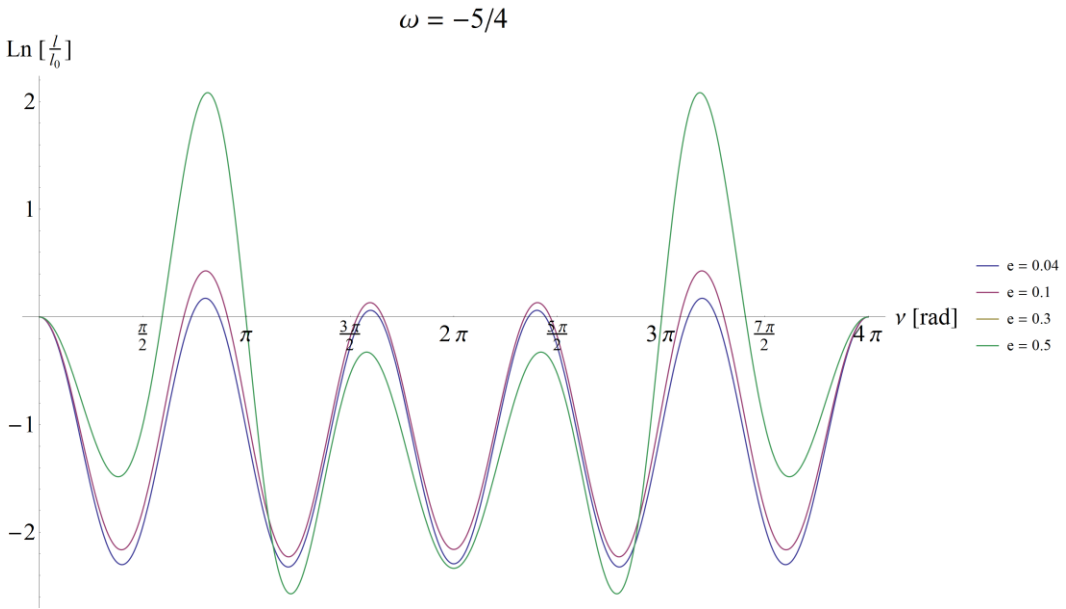

Figure A.2. 8 Tether logarithmic ratio for different eccentricities and $\omega = -5/4$

2.2 Permanent orientation

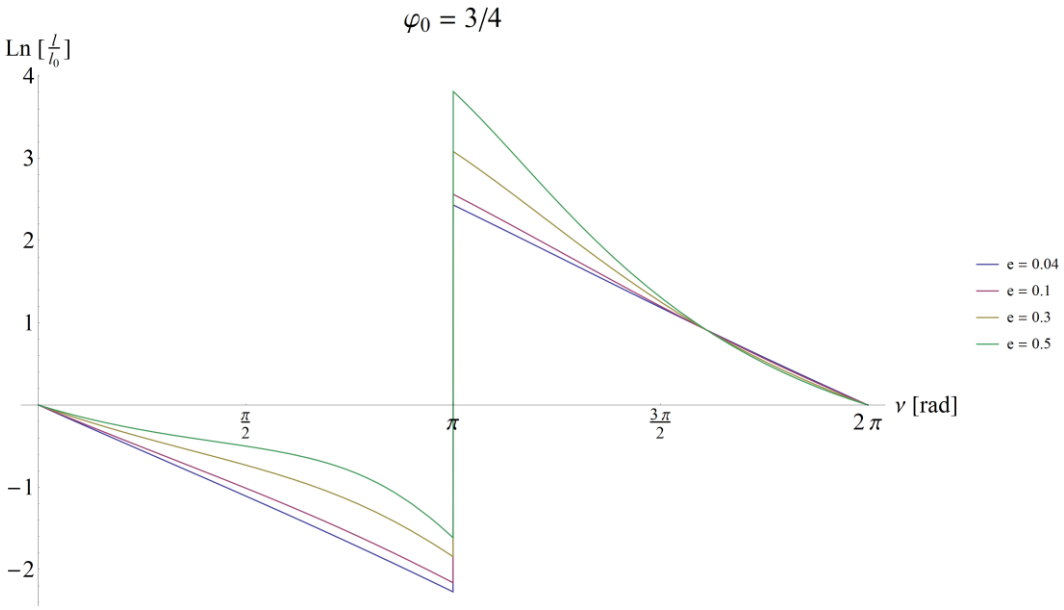

Figure A.2. 9 Tether logarithmic ratio for different eccentricities and $\omega = 3/4$

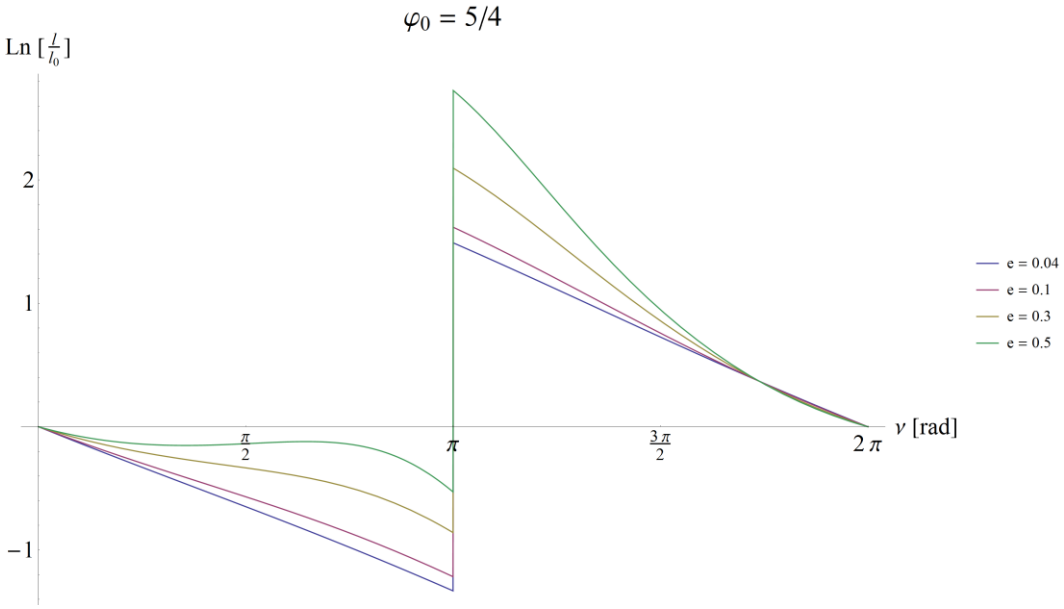

Figure A.2. 10 Tether logarithmic ratio for different eccentricities and $\omega = 5/4$

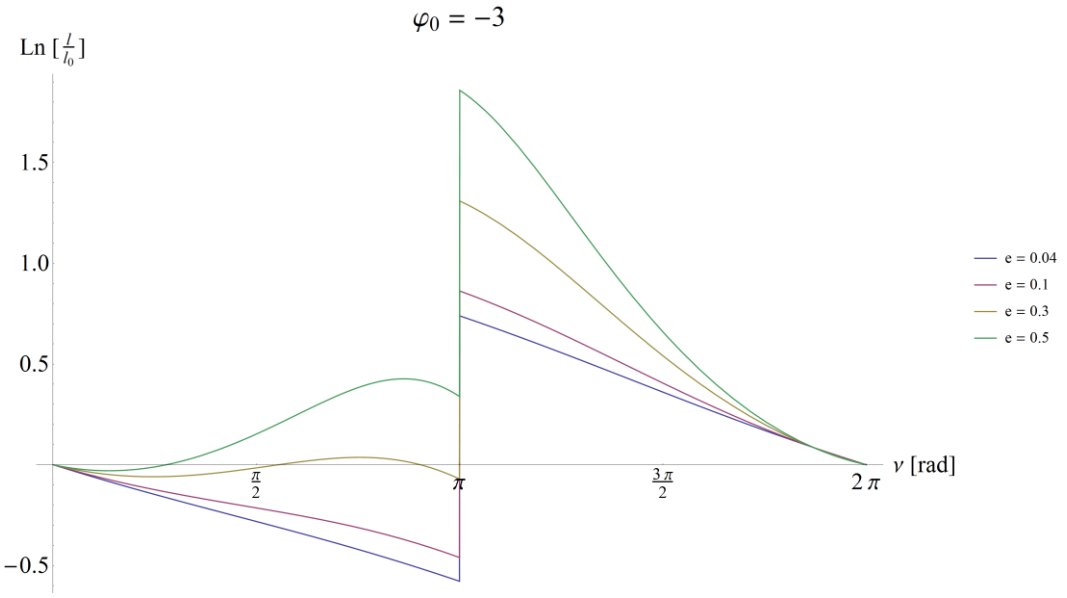

Figure A.2. 11 Tether logarithmic ratio for different eccentricities and $\omega = -3$

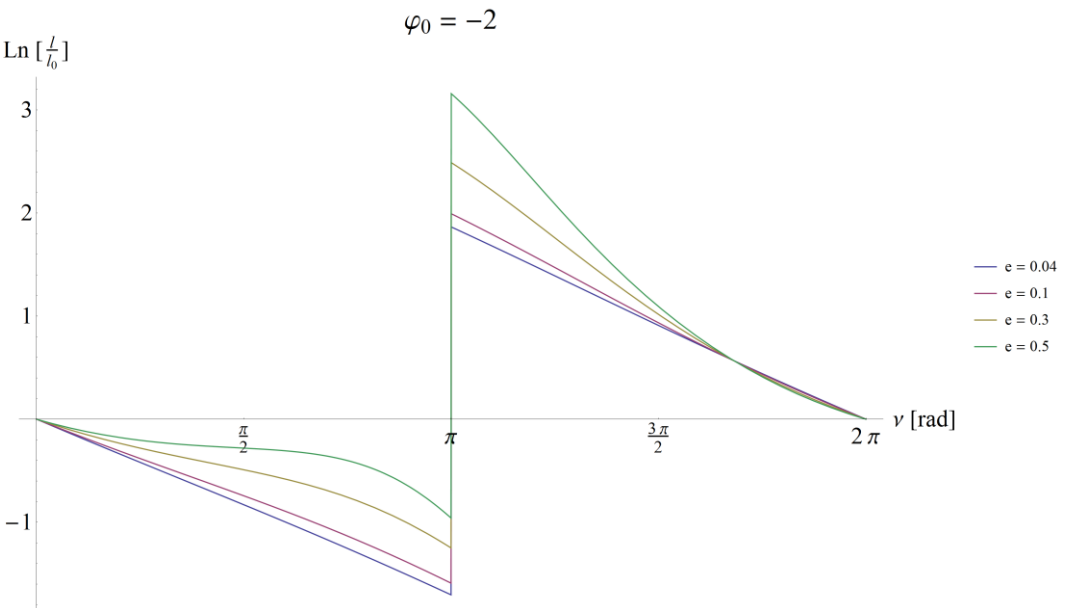

Figure A.2. 12 Tether logarithmic ratio for different eccentricities and $\omega = -2$

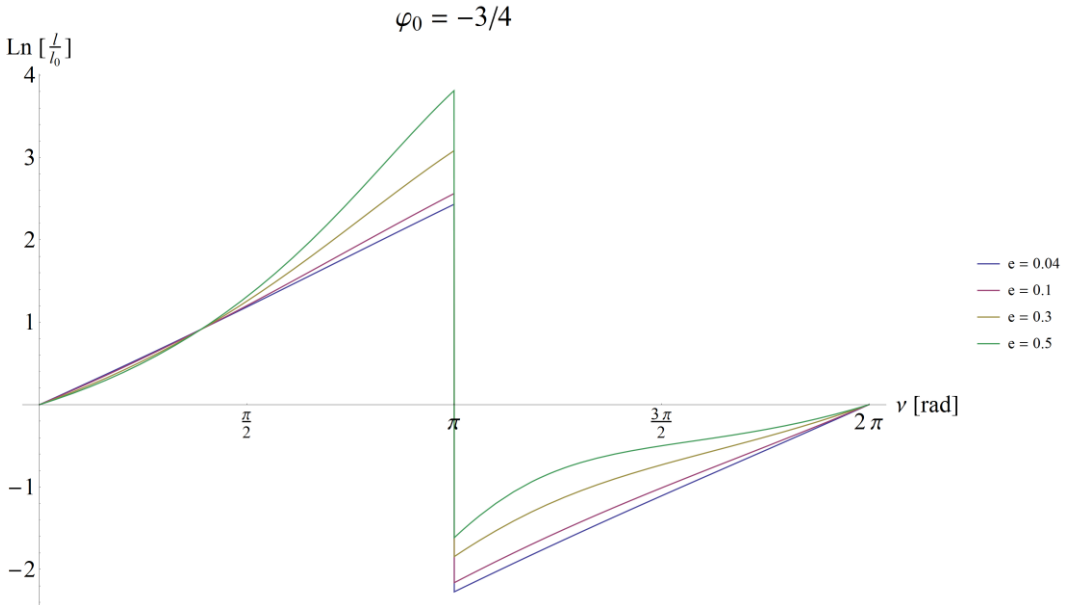

Figure A.2. 13 Tether logarithmic ratio for different eccentricities and $\omega = -3/4$

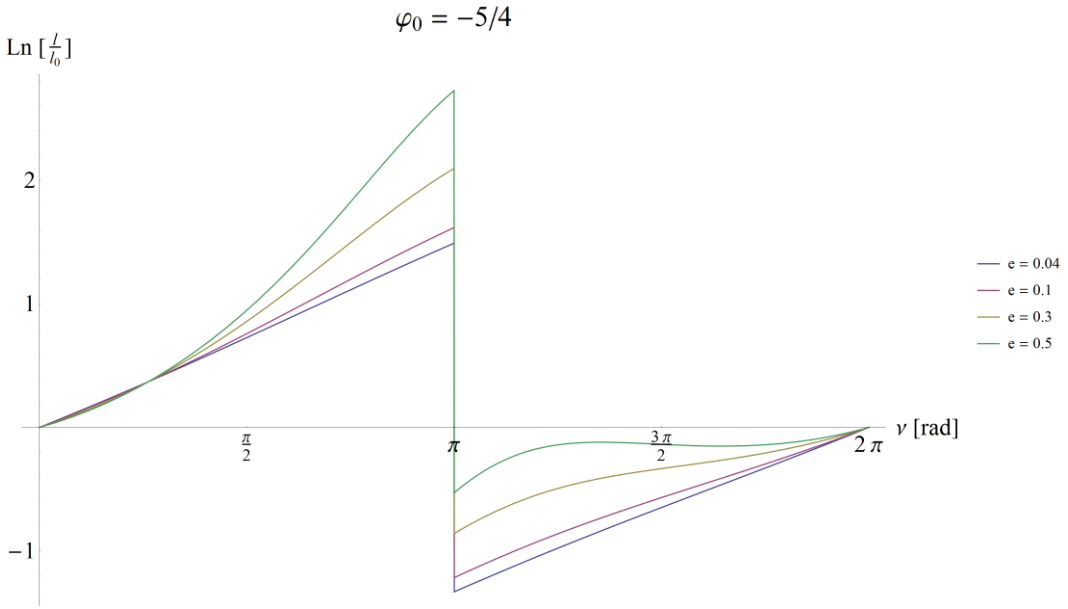

Figure A.2. 14 Tether logarithmic ratio for different eccentricities and $\omega = -5/4$